

EFFICIENT SIMULATION OF LÉVY-DRIVEN POINT PROCESSES

YAN QU,* AND

ANGELOS DASSIOS,* *London School of Economics and Political Science*

HONGBIAO ZHAO,** *Shanghai University of Finance and Economics*

Abstract

In this paper, we introduce a new large family of Lévy-driven point processes with (and without) contagion, by generalising the classical self-exciting Hawkes process and doubly stochastic Poisson processes with non-Gaussian Lévy-driven Ornstein–Uhlenbeck-type intensities. The resulting framework may possess many desirable features such as skewness, leptokurtosis, mean-reverting dynamics, and more importantly, the ‘contagion’ or feedback effects, which could be very useful for modelling event arrivals in finance, economics, insurance, and many other fields. We characterise the distributional properties of this new class of point processes and develop an efficient sampling method for generating sample paths exactly. Our simulation scheme is mainly based on the distributional decomposition of the point process and its intensity process. Extensive numerical implementations and tests are reported to demonstrate the accuracy and effectiveness of our scheme. Moreover, we use portfolio risk management as an example to show the applicability and flexibility of our algorithms.

Keywords: Contagion risk; portfolio risk management; Monte Carlo simulation; exact simulation; exact decomposition; self-exciting jump process with non-Gaussian Ornstein–Uhlenbeck intensity; point process; branching process; stochastic intensity model; non-Gaussian Ornstein–Uhlenbeck process; gamma process; inverse Gaussian subordinator; tempered stable subordinator

2010 Mathematics Subject Classification: Primary 60G55; 62E15; 65C05
Secondary 60E07; 60G51; 60J75

1. Introduction

Doubly stochastic Poisson processes or *Cox processes* [39, 40] have now been widely applied as survival or event timing models in many areas. Compared with a simple Poisson process, they are better able to capture event arrivals with complex dynamics structures. However, in reality, except for the impact from external factors, event arrivals may often present ‘contagion’, clustering, or feedback effects, such as social media sharing online, trade transactions in market microstructure, defaults in the credit market, jumps in investment returns, and loss claims in insurance businesses, to name a few. Das, Duffie, Kapadia, and Saita [44] and Duffie, Eckner, Horel, and Saita [55] provided evidence that Cox models, which are based on conditional independence assumption, cannot fully capture credit contagion.

Received 24 December 2018; revision received 10 June 2019.

* Postal address: Department of Statistics, London School of Economics and Political Science, Houghton Street, London WC2A 2AE, UK.

** Postal address: School of Statistics and Management, Shanghai University of Finance and Economics, 777 Guoding Road, Shanghai 200433, China; Shanghai Institute of International Finance and Economics, 777 Guoding Road, Shanghai 200433, China.

The phenomena of contagion became more evident in the credit market during the global financial crisis of 2007–2009 and the European debt crisis since the end of 2009; see [64]. A seminal framework tailored for modelling event contagion is the *Hawkes process* [70, 71]. It is a self-exciting point process where each arrival of events would trigger a simultaneous jump in its own intensity and hence more events follow. Empirical evidence and econometric analysis can be found in [20], [77], [41], [61], [60], [10], [7], [6], and [9]. Recently, it has been extended in the literature by being combined with Cox processes to enrich the model eligibility, in the sense that both internal and external impacts can be facilitated in one single framework; see [21], [22], [46], and [48].

Meanwhile, from a micro perspective, it is becoming more apparent that real financial data exhibit deviations from normality with the availability of high-frequency data; see [62] for a pioneering investigation into the high-frequency financial data, and [5] for recent advances in financial econometrics. Barndorff-Nielsen and Shephard [14, 15] have proposed a class of stochastic processes, namely *non-Gaussian Ornstein–Uhlenbeck (OU) models*, which have gained extensive popularity for modelling the non-normality presented in finance and economics. They could offer greater flexibility, and possess many crucial features, such as skewness, leptokurtosis and mean-reverting dynamics, which are often observed in financial markets; see [88] and [34] for empirical evidence. Moreover, this generality does not hinder their analytical tractability. In particular, they have become extremely popular for modelling stochastic volatilities; see [19], [14], [15], [16], [17], [18], and [29]. These stochastic volatility models have led to other applications such as derivative pricing and risk analysis; see [87] and [81]. On the other hand, these processes can serve as stochastic intensity models for event arrivals. For instance, they have been used to model irregularly spaced trade-by-trade intraday data, mortality rates in insurance, and default intensities for credit risk in finance; see [93], [30], [69], and [95]. In particular, for credit risk modelling, a mean-reverting OU intensity could be particularly useful for capturing business cycle effects on average industrial defaults, as obviously default rates would increase in a recession and decrease in a boom [59]. This is similar to the environment of interest rates, so defaults and the associated losses in the credit market often present a mean-reverting pattern; see [64] for detailed analysis and evidence from a long-term historical perspective. Duffie, Eckner, Horel, and Saita [55] also found a mean-reverting *frailty* that would influence US non-financial defaults. Moreover, empirical evidence shows that the tails of Gaussian distributions are often too thin to capture risk in the credit market, and fluctuations are often sudden and jump-like, driven by unexpected news announcements. The distribution of default rates is highly skewed towards large values [64]. Therefore, macroeconomic shocks powered by a Lévy-driven non-Gaussian process rather than a Gaussian process may be more appropriate for capturing the dynamic structure of default intensities in reality.

It is therefore natural for us to combine these main streamlines in the literature to form a unified and consistent framework. In this paper, we construct a new large family of Lévy-driven point processes, termed the *self-exciting jump process with non-Gaussian OU intensity*, or the *Lévy-driven contagion process*. It is fundamentally powered by a Lévy process. More precisely, its stochastic intensity is a positive non-Gaussian process with additional self-exciting jumps. It can also be defined as a *branching process* via the cluster process representation. Accordingly, the resulting models are analytically tractable, and they intrinsically inherit the great flexibility of the two original processes, as well as their desirable features, including skewness, leptokurtosis, mean-reverting dynamics, and more importantly, the ‘contagion’ or feedback effects. These newly constructed processes would then substantially enrich continuous-time models tailored for quantifying the ‘contagion’ of event arrivals in finance, economics, insurance, queueing and many other fields.

Simulation plays a crucial role in the implementation, simulation-based statistical inference and empirical studies for new models. For instance, for modelling credit risk in practice, events of extreme losses and defaults are rare, and data are scarce. The key quantities at the centre of financial risk management, such as the value at risk of an aggregate loss distribution for a heterogeneous portfolio, are often a lack of closed-form formulas. A simulation-based approach then becomes a standard technique. In particular, the *exact simulation* scheme is highly desirable as it has the primary advantage of generating sample paths according to the underlying process law exactly [24, 31]. To our knowledge, there is no exact simulation algorithms in the literature even for our important special cases, the non-Gaussian OU stochastic intensity models without contagion. We first propose a general sampling framework for exactly simulating Lévy-driven contagion processes based on the *decomposition technique*. This decomposition approach has also been recently used in [47] and [49] to simulate the classical Hawkes process and point process with CIR intensity, and in [50], [89], and [90] to simulate tempered stable distributions and gamma-driven Ornstein–Uhlenbeck processes. We then focus on exploiting some very typical specifications of Lévy processes such as the gamma process and the tempered stable subordinator, where remarkably the resulting point processes can be analytically decomposed into several types of basic components, each of which can be exactly simulated, either directly or via an *acceptance–rejection (A/R) scheme*. Even though the underlying process possesses a complex structure, neither truncation nor discretisation are required. Moreover, there is no numerical inversion for the cumulative distribution function (CDF) or Laplace (Fourier) transform.

The paper is organised as follows. Section 2 gives the mathematical definitions of this new family, and explains how they can be constructed from the classical non-Gaussian OU processes and the self-exciting point process. In Section 3 we develop a general framework for exactly sampling our new point processes. In Section 4 we derive the exact simulation algorithms based on the decomposition approach for two explicit cases when the driving Lévy processes are the gamma process and the tempered stable subordinator, respectively. Extensive numerical implementations and tests are reported in Section 5 to demonstrate the accuracy and effectiveness of our algorithms. Section 6 provides some financial applications to credit portfolio risk to show the applicability and flexibility of our algorithms. Finally, Section 7 draws a brief conclusion and suggests plenty of potential topics for future research based on this new framework.

2. Lévy-driven contagion models

In this section we construct a new framework for modelling event arrivals with contagion effects based on Lévy processes. That is, the intensity of the point process is set up to be a non-Gaussian OU process driven by a Lévy subordinator in cooperation with extra self-exciting jumps. Let us first define a simpler version without the self-exciting component.

Definition 2.1. (*Jump process with non-Gaussian intensity.*) A jump process with non-Gaussian intensity is a point process $N \equiv \{T_i\}_{i=1,2,\dots}$, i.e. $N_t = \sum_{i \geq 1} \mathbf{1}_{\{T_i \leq t\}}$ with the stochastic intensity λ_t satisfying the stochastic differential equation

$$d\lambda_t = -\delta\lambda_t dt + \rho dZ_t, \quad t \geq 0, \quad (2.1)$$

where

- $\rho > 0$ is an arbitrary positive constant,
- $\delta > 0$ is the constant rate of exponential decay,
- Z_t , with $Z_0 = 0$, is a Lévy subordinator, which is called the *background driving Lévy process* (BDLP) of a non-Gaussian OU process.

This is a special case of Cox point processes. A slightly mathematical generalisation, though very useful for applications, is to further incorporate a feedback mechanism in the framework by adding a series of self-exciting jumps, i.e. simultaneous jumps (or ‘co-jumps’), in the point process and its intensity process. More precisely, this new framework, as a generalised version of the jump process of Definition 2.1, is defined via the *stochastic intensity representation*, as follows.

Definition 2.2. (*Self-exciting jump process with non-Gaussian intensity.*) N_t is a *self-exciting jump process with non-Gaussian intensity*, if the intensity process of (2.1) is replaced by

$$d\lambda_t = -\delta\lambda_t dt + \rho dZ_t + dJ_t, \quad t \geq 0, \tag{2.2}$$

where the extra component J_t is a pure-jump process specified by

$$J_t := \sum_{i=1}^{N_t} X_i, \tag{2.3}$$

and $\{X_i\}_{i=1,2,\dots}$ are the sizes of *self-exciting jumps*, as the expression (2.3) reveals that the jumps simultaneously occur in the point process N_t and its intensity λ_t , and hence the arrivals of jumps trigger more jumps afterwards, with $\mathcal{F}_{T_i^-}$ -measurable distribution function $G(z)$, $z > 0$, occurring at the associated (ordered) arrival times $\{T_i\}_{i=1,2,\dots}$, respectively, and they are independent of Z_t . It means that the functional form of the distribution function $G(z)$ is revealed just before the arrival time T_i . This distribution could have a highly general dependence structure $G(z) = G(z | \cdot)$. For example, it could depend on the initial intensity λ_0 , the past history of intensity at or just before the jump arrival times $\{T_k\}_{k=1,2,\dots,i}$, all past jump sizes $\{X_k\}_{k=1,2,\dots,i-1}$, or the cumulated number of jumps N_t , and so on, as long as we can record this information, for example,

$$G(z) = G(z | T_1, T_2, \dots, T_i, \lambda_0, \lambda_{T_1^-}, \dots, \lambda_{T_i^-}, \lambda_{T_1}, \dots, \lambda_{T_{i-1}}).$$

This is similar to the *adaptive model* setting of [63], but it is different from the classical Hawkes process.

Similarly to the *Hawkes process* [72], N_t in Definition 2.2 can be equivalently redefined as a *branching process* via a *cluster process presentation* [43]. More precisely, N_t is a cluster point process which consists of two types of points: *immigrants* and their *offspring*. The arrivals of immigrants follow a Cox process with non-Gaussian OU intensity (2.1). Each immigrant generates its offspring, each offspring would generate further offspring, and so on. The generation of any offspring follows a Cox process with exponentially decaying intensity $X^* e^{-\delta(t-T^*)}$, where $X^* \stackrel{\mathcal{D}}{=} X_i$ and T^* is the arrival (birth) time of its previous generation. The superposition in [43] of all of these points forms our new self-exciting point process N_t with the stochastic intensity (2.2).

Note that, given the initial intensity level $\lambda_0 > 0$, the intensity process (2.2) can be equivalently expressed as

$$\lambda_t = \underbrace{\lambda_0 e^{-\delta t} + \rho \int_0^t e^{-\delta(t-s)} dZ_s}_{\text{exogenous commonly shared risk}} + \underbrace{\sum_{i=1}^{N_t} e^{-\delta(t-T_i)} X_i}_{\text{endogenous contagion risk}}, \quad t \geq 0,$$

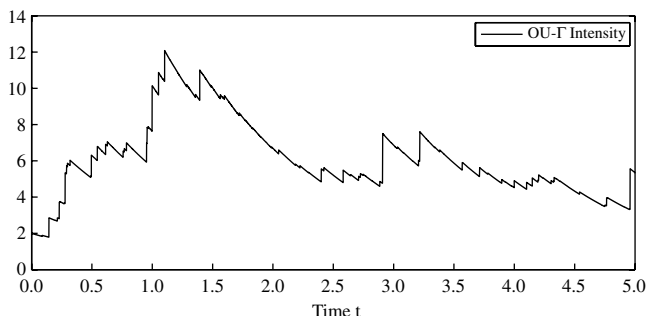


FIGURE 1: A sample path of interarrival intensity process (without self-exciting component) within the time period $t \in [0, 5]$ when the BDLP is a gamma process.

which is positive and càdlàg. In fact, this new framework integrates two major types of risk sources. For example, in the context of credit risk or systemic risk, the first part (i.e. the first two terms) is to model the cyclical dependence of companies on some exogenous risk (e.g. movements of interest or FX rates) commonly shared in the entire market, and the cyclical oscillation is captured by the mean-reverting non-Gaussian OU process; fundamental common shocks are captured by the pure-jump process Z_t . The second part (i.e. the last term) is to model the endogenous contagion risk due to the local interaction of companies in their business network, without which the overall risk would be underestimated.

The *interarrival intensity process* $\{\lambda_t\}_{T_i \leq t < T_{i+1}}$, for modelling exogenous commonly shared risk, is defined as the parts of intensity process excluding self-exciting jumps, i.e. (2.1), or

$$\lambda_t = e^{-\delta t} \lambda_0 + \rho \int_0^t e^{-\delta(t-s)} dZ_s, \quad t \in [T_i, T_{i+1}).$$

For instance, a sample path of the interarrival intensity process (without self-exciting component) within the time period $t \in [0, 5]$ when the BDLP is a gamma process is represented in Figure 1.

This framework is the generalisation of several classical models in the literature. If there are no self-exciting jumps, i.e. $X_i \equiv 0$ for any i , then the intensity process (2.2) is a *non-Gaussian OU process* [14, 15, 16, 17, 19]. If there is no BDLP Z_t , then the point process N_t is a generalised *Hawkes process* [70, 71] with random marks. If the BDLP Z_t is trivially a subordinator of compound Poisson, then N_t is a *dynamic contagion process* [46].

For notational simplicity, we denote the Lévy measure of BDLP Z_t by ν , the associated Laplace exponent and mean at unit time by

$$\Phi(u) := \int_0^\infty (1 - e^{-uy}) \nu(dy), \quad \mu_Z := \mathbb{E}[Z_1] = \int_0^\infty y \nu(dy), \quad u > 0,$$

the Laplace transform, mean of self-exciting jump sizes and a constant, respectively, by

$$\hat{g}(u) := \int_0^\infty e^{-uy} dG(y), \quad \mu_G := \int_0^\infty y dG(y), \quad \eta := \delta - \mu_G.$$

They are all assumed to be finite. In addition, we denote the $(i + 1)$ th interarrival time by

$$\tau_{i+1} := T_{i+1} - T_i, \quad i = 0, 1, 2, \dots, \quad T_0 = 0,$$

and the *cumulative intensity process* at time t by $\Lambda_t := \int_0^t \lambda_u du$.

One may be interested in their basic distributional properties such as means and Laplace transforms, and we provide some brief results for them in Appendix A with proofs. In particular, the conditional expectation of point process is provided here in Proposition 2.1, as it will be used later as a simple and general benchmark for numerically validating our newly developed simulation algorithms.

Proposition 2.1. (Conditional expectation of point process.) *The expectation of N_{t+s} conditional on N_t and λ_t is given by*

$$\mathbb{E}[N_{t+s} | N_t, \lambda_t] = \begin{cases} N_t + \frac{\rho\mu_Z}{\eta}s + \left(\lambda_t - \frac{\rho\mu_Z}{\eta}\right) \frac{1 - e^{-\eta s}}{\eta} & \eta \neq 0, \\ N_t + \lambda_t s + \frac{1}{2}\rho\mu_Z s^2 & \eta = 0, \end{cases} \quad s > 0.$$

3. General framework for exact simulation

In this section we outline an exact simulation framework based on exact distributional decomposition for a general point process of Lévy-driven non-Gaussian OU intensity *with* and *without* self-exciting jumps as defined in Definition 2.2 and 2.1, respectively. The entire simulation scheme can be decomposed into three major steps.

- (i) Conditional on the current arrival time T_i and the associated intensity level λ_{T_i} , generate the next interarrival time τ_{i+1} .
- (ii) Further conditional on the realisation of this interarrival time τ_{i+1} , generate the pre-jump intensity level $\lambda_{T_i+\tau_{i+1}^-}$ right before the next arrival time $T_{i+1} = T_i + \tau_{i+1}$.
- (iii) Add a self-exciting jump size X_{i+1} upon the intensity process λ_t and one unit in the point process N_t both at the next arrival time $T_{i+1} = T_i + \tau_{i+1}$.

By recursively implementing the three steps above, a full path of the point process N_t in any time horizon can be exactly produced without bias. A graphical illustration of this proposed algorithm design is provided in Figure 2.

The third step is in fact straightforward. In particular, if $X_{i+1} \equiv 0$ for any i , then it corresponds to the version *without* self-exciting jumps. In order to execute the first two steps, we have first to further investigate the joint distributional properties of the next interarrival time τ_{i+1} and the next pre-jump intensity level $\lambda_{T_i+\tau_{i+1}^-}$, which can be characterised by the conditional joint transform as follows.

Theorem 3.1. (Joint transform of pre-jump intensity and cumulative intensity.) *Conditional on the intensity level λ_{T_i} at the i th arrival time T_i , the joint transform of $(\lambda_{T_i+\tau^-}, \Lambda_{T_i+\tau} - \Lambda_{T_i})$ for any given period $\tau \in (0, \tau_{i+1})$ is given by*

$$\begin{aligned} & \mathbb{E}[e^{-v\lambda_{T_i+\tau^-}} e^{-(\Lambda_{T_i+\tau} - \Lambda_{T_i})} | \lambda_{T_i}] \\ &= \exp\left(-\left[\frac{1}{\delta} + \left(v - \frac{1}{\delta}\right)w\right]\lambda_{T_i} - \rho \int_v^{1/\delta+(v-1/\delta)w} \frac{\Phi(u)}{1-\delta u} du\right), \quad \tau \in (0, \tau_{i+1}), \end{aligned} \quad (3.1)$$

where $w := e^{-\delta\tau}$.

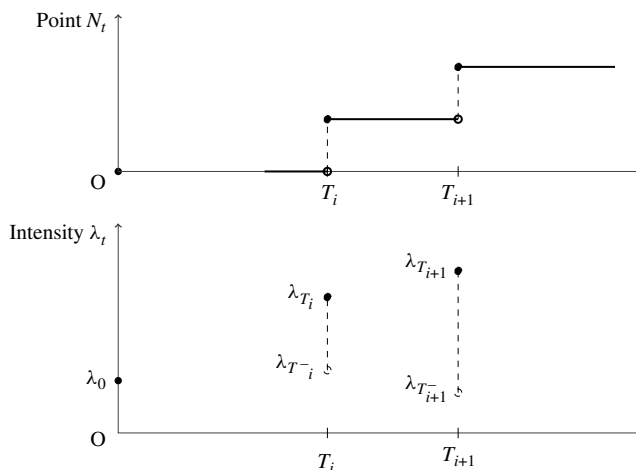


FIGURE 2: Exact simulation procedures for a path of point process N_t and the skeleton of its intensity process λ_t around the period $[T_i, T_{i+1}]$.

Proof. Given the i th arrival time T_i , the infinitesimal generator of (Λ, λ, t) within the period $t \in [T_i, T_i + \tau_{i+1})$ acting on any function $f(\Lambda, \lambda, t)$ within its domain $\Omega(\mathcal{A})$ is given by

$$\mathcal{A}f(\Lambda, \lambda, t) = \frac{\partial f}{\partial t} - \delta\lambda \frac{\partial f}{\partial \lambda} + \lambda \frac{\partial f}{\partial \Lambda} + \rho \left\{ \int_0^\infty [f(\Lambda, \lambda + y, t) - f(\Lambda, \lambda, t)] \nu(dy) \right\}. \quad (3.2)$$

Consider a function

$$f(\Lambda, \lambda, t) = e^{-\tilde{\nu}\Lambda} e^{-\lambda A(t)} e^{R(t)}, \quad \tilde{\nu} \in \mathbb{R}^+, \quad (3.3)$$

where $A(t)$ and $R(t)$ are deterministic and differentiable functions with respect to t . Substituting (3.3) into (3.2) and setting $\mathcal{A}f = 0$, we have

$$-\lambda A'(t) + R'(t) + \delta\lambda A(t) - \tilde{\nu}\lambda - \rho\Phi(A(t)) = 0.$$

Since this equation holds for any λ and Λ , it is equivalent to the equations

$$A'(t) = \delta A(t) - \tilde{\nu}, \quad R'(t) = \rho\Phi(A(t)).$$

Hence, for any time $t \in [T_i, T_i + \tau_{i+1})$, we have

$$A(t) = k e^{\delta t} - \tilde{\nu} \frac{e^{\delta t} - 1}{\delta}, \quad R(t) = \rho \int_0^t \Phi \left(k e^{\delta s} - \tilde{\nu} \frac{e^{\delta s} - 1}{\delta} \right) ds, \quad k \in \mathbb{R}^+.$$

By the basic property of infinitesimal generator in [45], we have the martingale

$$e^{-\tilde{\nu}\Lambda_t} \exp \left(- \left(k e^{\delta t} - \tilde{\nu} \frac{e^{\delta t} - 1}{\delta} \right) \lambda_t + \rho \int_0^t \Phi \left(k e^{\delta s} - \tilde{\nu} \frac{e^{\delta s} - 1}{\delta} \right) ds \right).$$

Setting $\tilde{\nu} = 1$ and $A(T_i + \tau^-) = v$ for any $\tau \in (0, \tau_{i+1})$ and using the martingale property, we have

$$\begin{aligned} & \mathbb{E}[e^{-v\lambda_{T_i+\tau^-}} e^{-(\Lambda_{T_i+\tau^-} - \Lambda_{T_i})} | \lambda_{T_i}] \\ &= \exp \left(- \left[\frac{1}{\delta} + \left(v - \frac{1}{\delta} \right) w \right] \lambda_{T_i} - \rho \int_0^\tau \Phi \left(\frac{1}{\delta} + \left(v - \frac{1}{\delta} \right) e^{-\delta s} \right) ds \right). \end{aligned}$$

Hence, we can immediately obtain (3.1) by the change of variable $u = 1/\delta + (v - 1/\delta)e^{-\delta s}$. □

Theorem 3.1 provides us with a crucial tool for further investigating the distributional properties of the interarrival time τ_{i+1} and the pre-jump intensity level $\lambda_{T_i+\tau_{i+1}^-}$, jointly and separately, which later leads to their efficient algorithms for exact simulation as follows. Note that, however, the main mathematical contribution of this paper is the *exact distributional decomposition* for our new point processes via Theorem 3.1 rather than deriving the transform in Theorem 3.1.

3.1. Exact simulation of interarrival time

Let us first outline how to simulate the interarrival time. Given the intensity level λ_{T_i} at the i th arrival time T_i , interestingly, the $(i + 1)$ th interarrival time τ_{i+1} can be exactly expressed as the minimum of two much simpler random variables $V_{T_i}^*$ and V^* , where

- (i) $V_{T_i}^*$ is a defective random variable, which can be directly generated by an explicit inverse transform,
- (ii) V^* is a well-defined random variable, which can be exactly simulated by a simplified version of the classical *thinning scheme* [79].

Algorithm 3.1. (*Exact simulation of interarrival time.*) Conditional on the intensity level λ_{T_i} , the next interarrival time τ_{i+1} can be exactly simulated via

$$\tau_{i+1} \stackrel{\mathcal{D}}{=} \begin{cases} V^* \wedge V_{T_i}^* & D_i > 0, \\ V^* & D_i < 0, \end{cases}$$

where

- D_i is simulated via

$$D_i := 1 + \frac{\delta}{\lambda_{T_i}} \ln U_1, \quad U_1 \sim \mathbf{U}[0, 1],$$

- $V_{T_i}^*$ is a simple defective random variable with $\mathbb{P}\{V_{T_i}^* = \infty\} = \exp(-\frac{1}{\delta}\lambda_{T_i})$,

$$V_{T_i}^* \stackrel{\mathcal{D}}{=} -\frac{1}{\delta} \ln D_i, \quad D_i > 0, \tag{3.4}$$

- V^* is the first arrival time of a non-homogeneous Poisson process with the rate function

$$\zeta_t := \rho \Phi(G_0(t)), \quad G_0(u) := \frac{1 - e^{-\delta u}}{\delta}, \quad u \geq 0, \tag{3.5}$$

and it can be exactly simulated via the simplified thinning scheme of Algorithm 3.2.

Proof. Setting $v = 0$ in (3.1) of Theorem 3.1, we have

$$\mathbb{P}\{\tau_{i+1} > \tau \mid \lambda_{T_i}\} = \mathbb{E}[e^{-(\Lambda_{T_i+\tau} - \Lambda_{T_i})} \mid \lambda_{T_i}] = \mathbb{P}\{V^* > \tau\} \times \mathbb{P}\{V_{T_i}^* > \tau\},$$

where

$$\mathbb{P}\{V^* > \tau\} = \exp\left(-\rho \int_0^\tau \Phi(G_0(u)) du\right), \quad \mathbb{P}\{V_{T_i}^* > \tau\} = e^{-G_0(\tau)\lambda_{T_i}}. \tag{3.6}$$

This implies that the next interarrival time τ_{i+1} conditional on the current intensity level λ_{T_i} can be expressed as the minimum of two independent random variables V^* and $V_{T_i}^*$. Note that

$V_{T_i}^*$ is a defective random variable that has a mass probability at the infinity, since the CDF of $V_{T_i}^*$ is

$$F_{V_{T_i}^*}(\tau) = 1 - e^{-G_0(\tau)\lambda_{T_i}},$$

with

$$F_{V_{T_i}^*}(\infty) = 1 - \exp\left(-\frac{1}{\delta}\lambda_{T_i}\right) < 1,$$

and the density $f_{V_{T_i}^*}(\tau) > 0$ for any $\tau > 0$. Obviously, if $D_i > 0$, then $V_{T_i}^*$ can be exactly simulated using the explicit inverse transform (3.4), whereas V^* can be interpreted as the first arrival time from a non-homogeneous Poisson process, and it can be exactly simulated via Algorithm 3.2 as follows. \square

Algorithm 3.2. (Simplified thinning scheme.) V^* can be exactly simulated by the following steps.

1. Initialise the candidate time $\tilde{t} = 0$.
2. Generate an exponential random variable $E^* \sim \text{Exp}(\zeta_\infty)$ where

$$\zeta_\infty := \lim_{t \rightarrow \infty} \zeta_t = \rho \Phi\left(\frac{1}{\delta}\right), \tag{3.7}$$

and set $\tilde{t} = \tilde{t} + E^*$.

3. Generate a uniform random variable $U_2 \sim \text{U}[0, 1]$,
 - if $U_2 \leq \zeta_{\tilde{t}}/\zeta_\infty$, then accept this candidate by setting $V^* = \tilde{t}$,
 - if $U_2 > \zeta_{\tilde{t}}/\zeta_\infty$, then reject this candidate, and go back to step 2 and continue.

Proof. Since ζ_t in (3.5) is a strictly increasing and concave function of time t with the initial value $\zeta_0 = 0$ at time $t = 0$, the maximum level is ζ_∞ . Then the algorithm above is in fact a simplified version of the classical *thinning scheme* [79] where only the first arrival time within the period of $[0, t]$ is recorded. \square

3.2. Exact simulation of pre-jump intensity level

Conditional on the realisation of interarrival time τ_{i+1} as generated by Algorithm 3.1, the Laplace transform of the next pre-jump intensity level $\lambda_{T_i+\tau_{i+1}^-}$ is provided as follows.

Theorem 3.2. (Laplace transform of pre-jump intensity.) *Conditional on the intensity level λ_{T_i} and the $(i + 1)$ th interarrival time τ_{i+1} , the Laplace transform of pre-jump intensity level*

$\lambda_{T_i+\tau_{i+1}^-}$ is given by

$$\begin{aligned} & \mathbb{E}[e^{-v\lambda_{T_i+\tau_{i+1}^-}} \mid \tau_{i+1} = \tau, \lambda_{T_i}] \\ &= e^{-v\lambda_{T_i}} \times \exp\left(-\rho \int_v^{1/\delta+(v-1/\delta)w} \frac{\Phi(u) - \Phi\left(u - \frac{u-1/\delta}{v-1/\delta}v\right)}{1-\delta u} du\right) \\ & \quad \times \frac{\frac{\rho}{\delta} \int_0^\infty e^{-vs} \int_s^{s/w} e^{s/\delta} e^{-y/\delta} \nu(dy) ds + w\lambda_{T_i}}{\frac{\rho}{\delta} \int_0^\infty \int_s^{s/w} e^{s/\delta} e^{-y/\delta} \nu(dy) ds + w\lambda_{T_i}}. \end{aligned} \tag{3.8}$$

Proof. Note that the density function of the $(i + 1)$ th interarrival time conditional on the intensity level λ_{T_i} is

$$\mathbb{P}\{\tau_{i+1} \in d\tau \mid \lambda_{T_i}\} = \mathbb{E}\left[\lambda_{T_i+\tau^-} \exp\left(-\int_{T_i}^{T_i+\tau} \lambda_u du\right) \mid \lambda_{T_i}\right] d\tau,$$

which implies that

$$\mathbb{E}\left[e^{-v\lambda_{T_i+\tau_{i+1}^-}} \mathbf{1}_{\{\tau_{i+1} \in d\tau\}} \mid \lambda_{T_i}\right] = \mathbb{E}\left[\lambda_{T_i+\tau^-} e^{-v\lambda_{T_i+\tau^-}} \exp\left(-\int_{T_i}^{T_i+\tau} \lambda_u du\right) \mid \lambda_{T_i}\right] d\tau.$$

Hence, we have

$$\mathbb{E}\left[e^{-v\lambda_{T_i+\tau_{i+1}^-}} \mid \tau_{i+1} = \tau, \lambda_{T_i}\right] = \frac{\mathbb{E}\left[\lambda_{T_i+\tau^-} e^{-v\lambda_{T_i+\tau^-}} e^{-(\Lambda_{T_i+\tau} - \Lambda_{T_i})} \mid \lambda_{T_i}\right]}{\mathbb{E}\left[\lambda_{T_i+\tau^-} e^{-(\Lambda_{T_i+\tau} - \Lambda_{T_i})} \mid \lambda_{T_i}\right]}. \tag{3.9}$$

The numerator of (3.9) can be obtained by differentiating the joint transform (3.1) with respect to v , that is,

$$\begin{aligned} & \mathbb{E}\left[\lambda_{T_i+\tau^-} e^{-v\lambda_{T_i+\tau^-}} e^{-(\Lambda_{T_i+\tau} - \Lambda_{T_i})} \mid \lambda_{T_i}\right] \\ &= -\frac{\partial}{\partial v} \mathbb{E}\left[e^{-v\lambda_{T_i+\tau^-}} e^{-(\Lambda_{T_i+\tau} - \Lambda_{T_i})} \mid \lambda_{T_i}\right] \\ &= -\frac{\partial}{\partial v} \left[\exp\left(-\left[\frac{1}{\delta} + \left(v - \frac{1}{\delta}\right) e^{-\delta\tau}\right] \lambda_{T_i}\right) \right. \\ & \quad \left. \times \exp\left(-\rho \int_0^\tau \Phi\left(\frac{1}{\delta} + \left(v - \frac{1}{\delta}\right) e^{-\delta u}\right) du\right) \right] \\ &= -\frac{\partial}{\partial v} \left[e^{-G_v(\tau)\lambda_{T_i}} \times e^{-\rho F_v(\tau)} \right] \\ &= -\left[\rho \frac{\partial}{\partial v} F_v(\tau) + \frac{\partial}{\partial v} G_v(\tau) \right] \times e^{-G_v(\tau)\lambda_{T_i}} e^{-\rho F_v(\tau)}, \end{aligned}$$

where

$$G_v(u) := \frac{1}{\delta} + \left(v - \frac{1}{\delta}\right) e^{-\delta u}, \quad F_v(\tau) := \int_0^\tau \Phi(G_v(u)) du,$$

and

$$\begin{aligned} \frac{\partial}{\partial v} G_v(\tau) &= -\lambda_{T_i} e^{-\delta\tau}, \\ \frac{\partial}{\partial v} F_v(\tau) &= \int_0^\tau \int_0^\infty y e^{-\delta u} e^{-[1/\delta+(v-1/\delta)e^{-\delta u}]y} \nu(dy) du. \end{aligned}$$

Note that ν is the Lévy measure for a general BDLP Z_t , so we have

$$\begin{aligned} &\mathbb{E}\left[e^{-\nu\lambda_{T_i+\tau_{i+1}^-} | \tau_{i+1} = \tau, \lambda_{T_i}}\right] \\ &= \frac{\left(\rho \int_0^\tau \int_0^\infty y e^{-\delta u} e^{-[1/\delta+(v-1/\delta)e^{-\delta u}]y} \nu(dy) du + w\lambda_{T_i}\right) \times e^{-G_v(\tau)\lambda_{T_i}} e^{-\rho F_v(\tau)}}{\left(\rho \int_0^\tau \int_0^\infty y e^{-\delta u} e^{-(1/\delta)(1-e^{-\delta u})y} \nu(dy) du + w\lambda_{T_i}\right) \times e^{-G_0(\tau)\lambda_{T_i}} e^{-\rho F_0(\tau)}} \\ &= \frac{\rho \int_0^\tau \int_0^\infty y e^{-\delta u} e^{-[1/\delta+(v-1/\delta)e^{-\delta u}]y} \nu(dy) du + w\lambda_{T_i}}{\rho \int_0^\tau \int_0^\infty y e^{-\delta u} e^{-(1/\delta)(1-e^{-\delta u})y} \nu(dy) du + w\lambda_{T_i}} \\ &\quad \times \frac{\mathbb{E}\left[e^{-\nu\lambda_{T_i+\tau^-}} e^{-(\Lambda_{T_i+\tau}-\Lambda_{T_i})} | \lambda_{T_i}\right]}{\mathbb{E}\left[e^{-(\Lambda_{T_i+\tau}-\Lambda_{T_i})} | \lambda_{T_i}\right]}. \end{aligned} \tag{3.10}$$

The first term of (3.10) can be calculated more explicitly as

$$\begin{aligned} &\frac{\rho \int_0^\tau \int_0^\infty y e^{-\delta u} e^{-[1/\delta+(v-1/\delta)e^{-\delta u}]y} \nu(dy) du + w\lambda_{T_i}}{\rho \int_0^\tau \int_0^\infty y e^{-\delta u} e^{-(1/\delta)(1-e^{-\delta u})y} \nu(dy) du + w\lambda_{T_i}} \\ &= \frac{\rho \int_v^{1/\delta+(v-1/\delta)w} \int_0^\infty y \frac{u-1/\delta}{v-1/\delta} e^{-uy} \nu(dy) \frac{du}{1-\delta u} + w\lambda_{T_i}}{\rho \int_v^{1/\delta+(v-1/\delta)w} \int_0^\infty y \frac{u-1/\delta}{v-1/\delta} e^{-(u-u-1/\delta/v-1/\delta)v} \nu(dy) \frac{du}{1-\delta u} + w\lambda_{T_i}} \\ &= \frac{\frac{\rho}{1-\delta v} \int_v^{1/\delta+(v-1/\delta)w} \int_0^\infty y e^{-(u-1/\delta)y} e^{-y/\delta} \nu(dy) du + w\lambda_{T_i}}{\frac{\rho}{1-\delta v} \int_v^{1/\delta+(v-1/\delta)w} \int_0^\infty y e^{-(u-(1/\delta-\frac{u-1/\delta}{v-1/\delta}v)y} e^{-y/\delta} \nu(dy) du + w\lambda_{T_i}} \\ &= \frac{-\frac{\rho}{\delta} \int_{1-\delta v}^{(1-\delta v)w} \int_0^\infty y e^{((1-\delta v)zy)/\delta} e^{-y/\delta} \nu(dy) dz + w\lambda_{T_i}}{-\frac{\rho}{\delta} \int_{1-\delta v}^{(1-\delta v)w} \int_0^\infty y e^{zy/\delta} e^{-y/\delta} \nu(dy) dz + w\lambda_{T_i}} \\ &= \frac{\frac{\rho}{\delta} \int_0^\infty e^{-\nu s} \int_s^{s/w} e^{s/\delta} e^{-y/\delta} \nu(dy) ds + w\lambda_{T_i}}{\frac{\rho}{\delta} \int_0^\infty \int_s^{s/w} e^{s/\delta} e^{-y/\delta} \nu(dy) ds + w\lambda_{T_i}}. \end{aligned} \tag{3.11}$$

The denominator of the second term of (3.10) can also be obtained nicely by setting $\nu = 0$ in the joint transform (3.1), that is,

$$\mathbb{E}\left[e^{-(\Lambda_{T_i+\tau}-\Lambda_{T_i})} \mid \lambda_{T_i}\right] = \exp\left(-\frac{1-w}{\delta}\lambda_{T_i} - \rho \int_{\nu}^{1/\delta+(v-1/\delta)w} \frac{\Phi\left(u - \frac{u-1/\delta}{v-1/\delta}\nu\right)}{1-\delta u} ds\right).$$

Therefore the second term of (3.10) can be expressed by

$$\begin{aligned} & \frac{\mathbb{E}\left[e^{-\nu\lambda_{T_i+\tau^-}} e^{-(\Lambda_{T_i+\tau}-\Lambda_{T_i})} \mid \lambda_{T_i}\right]}{\mathbb{E}\left[e^{-(\Lambda_{T_i+\tau}-\Lambda_{T_i})} \mid \lambda_{T_i}\right]} \\ &= \frac{\exp\left(-\left[\frac{1}{\delta} + \left(v - \frac{1}{\delta}\right)w\right]\lambda_{T_i}\right) \exp\left(-\rho \int_{\nu}^{1/\delta+(v-1/\delta)w} \frac{\Phi(u)}{1-\delta u} du\right)}{\exp\left(-\frac{1}{\delta}(1-w)\lambda_{T_i}\right) \exp\left(-\rho \int_{\nu}^{1/\delta+(v-1/\delta)w} \frac{\Phi\left(u - \frac{u-1/\delta}{v-1/\delta}\nu\right)}{1-\delta u} du\right)} \\ &= e^{-\nu w\lambda_{T_i}} \times \exp\left(-\rho \int_{\nu}^{1/\delta+(v-1/\delta)w} \frac{\Phi(u) - \Phi\left(u - \frac{u-1/\delta}{v-1/\delta}\nu\right)}{1-\delta u} du\right). \end{aligned} \tag{3.12}$$

Finally, we obtain (3.8) immediately by combining the results from (3.11) and (3.12). □

Apparently, given the i th arrival time T_i and the $(i + 1)$ th interarrival time τ_{i+1} , the pre-jump intensity level $\lambda_{T_i+\tau_{i+1}^-}$ can be simulated by the numerical inversion of the Laplace transform (3.8) for any Lévy-driven contagion process once the associated Lévy measure ν (and the Laplace exponent Φ) are specified. Indeed, exact simulation for stochastic processes based on the numerical inversion of the Laplace or Fourier transforms has been widely adopted in the literature; see [24], [66], [32], [28], and [74].

However, for some subclasses such as the very popular specifications of gamma and tempered stable BDLPs, quite remarkably, based on Theorem 3.2 the pre-jump intensity level can be exactly decomposed into several simple elements, each of which can easily be simulated exactly without any numerical inversion procedure. In fact, this exact decomposition approach appropriately breaks the Lévy measure of the subordinator, and thereby it can be achieved by developing an exact distributional decomposition through Laplace-transform representations. In this paper, our focus is mainly on this decomposition approach, as it leads to a very efficient simulation algorithm for exactly sampling the whole point process, and more importantly, it does not involve additional discretisation or truncation errors which are inevitable in the numerical inversion approach. We will present our discovery based on the decomposition approach in much more detail later in Section 4.

3.3. Exact simulation of self-exciting jumps

Based on our key results of Algorithm 3.1 for the interarrival time τ_{i+1} and Theorem 3.2 for the associated pre-jump intensity level $\lambda_{T_i+\tau_{i+1}^-}$, it is now straightforward to integrate the self-exciting jumps further as the final step.

Algorithm 3.3. (*Exact simulation of self-exciting jumps.*) Conditional on (λ_{T_i}, T_i) for any step index $i \in \mathbb{N}^+$, the next self-exciting jumps occurring simultaneously in the intensity process and the point process can be exactly simulated via the following steps.

1. Simulate the $(i + 1)$ th interarrival time τ_{i+1} by thinning via Algorithm 3.1.
2. Set the $(i + 1)$ th arrival time by $T_{i+1} = T_i + \tau_{i+1}$.
3. Simulate the $(i + 1)$ th pre-jump intensity $\lambda_{T_{i+1}^-}$ by numerical inversion or exact decomposition for its Laplace transform in Theorem 3.2.
4. Add a self-exciting jump of size X_{i+1} to the intensity process at the $(i + 1)$ th arrival time T_{i+1} , i.e.

$$\lambda_{T_{i+1}} = \lambda_{T_{i+1}^-} + X_{i+1}. \tag{3.13}$$

5. Add one unit to the point process at the $(i + 1)$ th arrival time T_{i+1} , i.e. $N_{T_{i+1}} = N_{T_{i+1}^-} + 1$.

By recursively implementing Algorithm 3.3, the skeleton of any non-Gaussian OU intensity process λ_t and the associated full path of point process N_t in continuous time can be exactly generated. Moreover, there is almost no restriction on the size of self-exciting jump, X_{i+1} . It is very flexible as long as it does not overshoot the zero bound: it could be a constant, or a random variable with highly general dependence on the information before and at the arrival time T_i .

Overall, the whole process can be decomposed into interarrival times, pre-jump intensity levels and self-exciting jumps. In general, each of the pre-jump intensity levels in step 3 can be simulated in general by numerically inverting (3.8) using the Fourier inversion technique, once we specify a subordinator for the BDLP Z_t . However, for some subclasses, even the numerical inversion can be avoided. That is, the pre-jump intensity allows a further exact distributional decomposition, which leads to an exact simulation algorithm without numerical inversion. The resulting scheme thereby has no bias or truncation errors.

4. Typical examples: gamma and tempered stable contagion models

For model implementation, one needs to further specify the BDLP in an explicit form. Probably the most widely used and representative Lévy subordinators in the literature are the gamma process and the *tempered stable (TS) subordinator*. The term *tempered stable* in the context sometimes refers to *exponential tilted stable* (see [94] and [92] for more information). More precisely, they are two typical examples of Lévy processes with stationary, independent, and non-negative increments starting at 0 with finite variation and *infinite activity*, which means that there are infinitely many small jumps within any finite time interval (for some strong evidence from financial data see [80], [3], [4], and [78]); these processes behave very differently from the trivial case of compound Poisson process. Because of this nature, they cannot be simulated exactly by traditional methods for discretising sample paths. We provide the definitions for them using the Lévy measures (4.1) and (4.3) in Definitions 4.1 and 4.2, respectively.

Definition 4.1. (*Gamma distribution and gamma process.*) The gamma distribution with shape parameter a and rate parameter b , denoted by $\text{Gamma}(a, b)$, has the density function

$$f_{\text{Gamma}(a,b)}(s) = \frac{b^a}{\Gamma(a)} s^{a-1} e^{-bs}, \quad s > 0, \quad a, b > 0,$$

where $\Gamma(\cdot)$ is the *gamma function*, i.e. $\Gamma(u) := \int_0^\infty s^{u-1} e^{-s} ds$. The gamma process $\{G_t, t \geq 0\}$ is a pure-jump increasing Lévy process with independently gamma-distributed increments satisfying $G_1 \sim \text{Gamma}(a, b)$, $G_0 = 0$, and it has Lévy measure

$$\nu(ds) = as^{-1} e^{-bs} ds, \tag{4.1}$$

and the Laplace exponent

$$\Phi(u) = a \ln \left(1 + \frac{u}{b} \right), \tag{4.2}$$

and the mean at unit time

$$\mu_Z = \mathbb{E}[Z_1] = \frac{a}{b}.$$

The gamma distribution, as a well-known *right-skewed distribution*, is approximated by a normal distribution when its mean is large, and it has many computational conveniences. A well-known convenience, similar to the normal distribution, is that if $\{Y_i\}_{i=1,2,\dots,m}$ are independent, identically distributed (i.i.d.) random variables following a gamma distribution with mean μ_Y and variance σ_Y^2 , then the sum $\sum_{i=1}^m Y_i$ is gamma-distributed with mean $m\mu_Y$ and variance $m\sigma_Y^2$. Thus it is a very useful building block as the risk driver. Therefore, we provide applications for the gamma-contagion model later in Section 6.

Definition 4.2. (*Tempered stable (TS) distribution and tempered stable (TS) subordinator.*) The *positive tempered stable (TS) distribution*, abbreviated as $\text{TS}(\alpha, \beta, \theta)$, is defined by its Lévy measure

$$\nu(dy) = \frac{\theta}{y^{\alpha+1}} e^{-\beta y} dy, \quad y \geq 0, \quad \alpha \in (0, 1), \quad \beta, \theta \in \mathbb{R}^+, \tag{4.3}$$

with the *Laplace exponent*

$$\Phi(u) = -\theta \Gamma(-\alpha) [(\beta + u)^\alpha - \beta^\alpha], \tag{4.4}$$

the mean at unit time

$$\mu_Z = \mathbb{E}[Z_1] = \theta \beta^{\alpha-1} \Gamma(1 - \alpha),$$

where α is the stability index, θ is the intensity parameter, and β is the tilting parameter. The tempered stable (TS) subordinator is a Lévy process $\{Z_t : t \geq 0\}$ such that $Z_1 \sim \text{TS}(\alpha, \beta, \theta)$ for $0 < \alpha < 1$ and $\beta, \theta > 0$.

In fact, tempered stable distribution with three parameters is a very general and flexible distribution. The stable index α determines the importance of small jumps for the process trajectories, the intensity parameter θ controls the intensity of jumps, and the tilting parameter β determines the decay rate of large jumps. In particular, if $\alpha = 1/2$, it reduces to a very important distribution, the *inverse Gaussian (IG) distribution*, which can be interpreted as the distribution of the first passage time of a Brownian motion to an absorbing barrier. So, this family of tempered stable subordinators in Definition 4.2 also covers the *inverse Gaussian (IG) subordinator* as an important special case [11, 12]. Conventionally, the IG distribution is denoted by $\text{IG}(\mu_{\text{IG}}, \lambda_{\text{IG}})$, where μ_{IG} is the *mean parameter* and λ_{IG} is the *rate parameter*; see [33] for a detailed introduction to IG distributions. The IG subordinator is a special TS subordinator such that the BDLP $Z_t \sim \text{IG}(t/c, t^2)$ for any $c, t \in \mathbb{R}^+$, that is,

$$\text{IG} \left(\frac{t}{c}, t^2 \right) \stackrel{\mathcal{D}}{=} \text{TS} \left(\frac{1}{2}, \frac{c^2}{2}, \frac{t}{\sqrt{2\pi}} \right).$$

Many scholars have adopted gamma, inverse Gaussian, and tempered stable subordinators as the building blocks to further construct other useful stochastic processes, and there are tremendous relevant papers and work in the literature; see [14, 15, 17], [35], [76], [95],

and [81], to name a few. Their main attraction is that the resulting models could possess skewness and leptokurtosis marginally, while remaining highly mathematically tractable. Our new models introduced in this paper can additionally incorporate the ‘contagion’ property, which is also very desirable from the perspective of applications.

Exact simulation of interarrival time. For each case, the interarrival time can be simulated via the general algorithm of thinning scheme, Algorithm 3.2, by simply calculating ζ_∞ in (3.7) from (3.5) explicitly as

$$\zeta_\infty = \begin{cases} \rho a \ln \left(1 + \frac{1}{\delta b} \right) & \text{for gamma,} \\ -\rho \theta \Gamma(-\alpha) \left[\left(\beta + \frac{1}{\delta} \right)^\alpha - \beta^\alpha \right] & \text{for TS.} \end{cases}$$

Exact simulation of pre-jump intensity. The pre-jump intensity level conditional on the realisation of interarrival time is characterised by the Laplace transforms (3.8) in Theorem 3.2, with Lévy measures ν and Laplace exponents Φ specified by (4.1)–(4.2) and (4.3)–(4.4) for the gamma and TS cases, respectively. For both cases, the integral transforms of the pre-jump intensity levels can in fact be broken down into several simple elements.

The Laplace transform of pre-jump intensity level with three terms in (3.8) in fact consists of two parts: (3.11) and (3.12). Strikingly, based on Theorem 3.2, the first two terms of (3.8), i.e. (3.12), can be further exactly decomposed for the specified TS and gamma cases, respectively, as follows.

Algorithm 4.1. (*Exact simulation of pre-jump intensity level for Γ -contagion.*) For the Γ -contagion, conditional on the intensity level λ_{T_i} and the realisation of the $(i + 1)$ th interarrival time $\tau_{i+1} = \tau$, the distribution of the $(i + 1)$ th pre-jump intensity level $\lambda_{T_i+\tau^-}$ can be exactly decomposed by

$$\lambda_{T_i+\tau^-} \mid \lambda_{T_i} \stackrel{\mathcal{D}}{=} w\lambda_{T_i} + \tilde{\Gamma} + \tilde{B} \times S + \sum_{j=1}^{\tilde{N}} S_j, \tag{4.5}$$

where $\tilde{\Gamma}$, \tilde{B} , S , \tilde{N} and $\{S_j\}_{j=1,2,\dots}$ are all independent of each other,

- $\tilde{\Gamma}$ is a gamma random variable of

$$\tilde{\Gamma} \sim \text{Gamma} \left(-\frac{a\rho}{\delta} \ln w, \frac{\vartheta}{w} - \frac{1}{\delta} \right), \quad \vartheta := b + \frac{1}{\delta},$$

- \tilde{B} is a Bernoulli random variable taking 0 with probability p_1 and 1 with probability p_2 , and

$$p_1 = \frac{w\lambda_{T_i}}{(a\rho/\delta)C + w\lambda_{T_i}}, \quad p_2 = \frac{(a\rho/\delta)C}{(a\rho/\delta)C + w\lambda_{T_i}}, \quad C := \delta \ln \left(\frac{b\delta + 1 - w}{b\delta} \right),$$

- S is an exponential random variable of $S \sim \text{Exp}(\vartheta W_0 - 1/\delta)$ and

$$W_0 \stackrel{\mathcal{D}}{=} [1 - b\delta(e^{(C/\delta)U_0} - 1)]^{-1}, \quad U_0 \sim \text{U}[0, 1], \tag{4.6}$$

- \tilde{N} is a Poisson random variable of rate $(a\rho/\delta)\vartheta C_w$ and

$$C_w := \int_1^{1/w} \frac{\ln u}{\vartheta u - 1/\delta} du,$$

- $\{S_j\}_{j=1,2,\dots}$ are i.i.d. with $S_j \sim \text{Exp}(\vartheta W - 1/\delta)$, and W can be exactly simulated via the A/R scheme of Algorithm B.1.

Proof. In fact, Algorithm 4.1 is only an explicit specification of Theorem 3.2. Let us first calculate the first two terms of (3.8), i.e. (3.12), by

$$\begin{aligned} & \frac{\mathbb{E}\left[e^{-v\lambda_{T_i+\tau^-}} e^{-(\Lambda_{T_i+\tau^-} - \Lambda_{T_i})} \mid \lambda_{T_i}\right]}{\mathbb{E}\left[e^{-(\Lambda_{T_i+\tau^-} - \Lambda_{T_i})} \mid \lambda_{T_i}\right]} \\ &= e^{-vw\lambda_{T_i}} \times \exp\left(-\frac{a\rho}{\delta} \ln\left(\frac{1}{w}\right) \int_0^\infty (1 - e^{-vs})s^{-1} e^{-(\vartheta/w - 1/\delta)s} ds\right) \\ & \quad \times \exp\left(-\frac{a\vartheta\rho}{\delta} \int_0^\infty (1 - e^{-vs}) \int_1^{1/w} \left(\vartheta u - \frac{1}{\delta}\right) e^{-(\vartheta u - 1/\delta)s} \frac{\ln u}{\vartheta u - 1/\delta} du ds\right). \end{aligned}$$

Then, by calculating the whole equation (3.8) more explicitly, the conditional Laplace transform of the pre-jump intensity level $\lambda_{T_i+\tau^-}$ can be decomposed into four parts:

$$\begin{aligned} & \mathbb{E}\left[e^{-v\lambda_{T_i+\tau_i^-}} \mid \tau_{i+1} = \tau, \lambda_{T_i}\right] \\ &= e^{-vw\lambda_{T_i}} \times \exp\left(-\frac{\rho}{\delta} \ln\left(\frac{1}{w}\right) \int_0^\infty (1 - e^{-vs})s^{-1} e^{-(\theta/w - 1/\delta)s} ds\right) \\ & \quad \times \exp\left(-\frac{a\vartheta\rho}{\delta} \int_0^\infty (1 - e^{-vs}) \int_1^{1/w} \left(\vartheta u - \frac{1}{\delta}\right) e^{-(\vartheta u - 1/\delta)s} \frac{\ln u}{\vartheta u - 1/\delta} du ds\right) \\ & \quad \times \frac{a\rho C/\delta}{a\rho C/\delta + w\lambda_{T_i}} \\ & \quad \times \left[\int_0^\infty e^{-vs} \int_1^{1/w} \left(\vartheta u + \frac{1}{\delta}\right) e^{-(\vartheta u - 1/\delta)s} \frac{1}{C(\vartheta u^2 - 1/\delta u)} du ds + \frac{w\lambda_{T_i}}{a\rho C/\delta + w\lambda_{T_i}}\right]. \end{aligned} \tag{4.7}$$

This decomposition of (4.7) indicates that the conditional distribution of $\lambda_{T_i+\tau^-}$ is the sum of four independent simple elements of (4.5): (i) one deterministic trend, (ii) one random variable $\tilde{B} \times S$, (iii) one gamma random variable, and (iv) one compound Poisson random variable. Note that $\tilde{B} \times S$ can be alternatively defined as just one single random variable by

$$\tilde{B} \times S \stackrel{\mathcal{D}}{=} \begin{cases} 0 & \text{with probability } p_1 = \frac{w\lambda_{T_i}}{(a\rho/\delta)C + w\lambda_{T_i}}, \\ S \sim \text{Exp}\left(\vartheta W_0 - \frac{1}{\delta}\right) & \text{with probability } p_2 = \frac{(a\rho/\delta)C}{(a\rho/\delta)C + w\lambda_{T_i}}. \end{cases}$$

The CDF of W_0 is

$$F_{W_0}(u) = \frac{1}{C_w(a + 1/\delta)} \ln\left(\frac{(a + 1/\delta)u - 1/\delta}{a}\right), \quad u \in \left[1, \frac{1}{w}\right],$$

which can be inverted explicitly, so we have (4.6). The compound Poisson random variable $\sum_{j=1}^{\tilde{N}} S_j$ has the Laplace transform

$$\exp\left(-\frac{a\vartheta\rho}{\delta}C_w \int_0^\infty (1 - e^{-vs}) \int_1^{1/w} \left(\vartheta u - \frac{1}{\delta}\right) e^{-(\vartheta u - 1/\delta)s} \frac{\ln u}{C_w(\vartheta u - 1/\delta)} du ds\right),$$

so the Poisson rate is $a\vartheta\rho/\delta C_w$, and jump-sizes $\{S_j\}_{j=1,2,\dots}$ follow an exponential distribution with rate $(\vartheta W - 1/\delta)$. Here, W is a well-defined random variable with density (B.1), which can be exactly simulated via the A/R scheme of Algorithm B.1. For more details on designing simulation algorithms based on the A/R mechanism, see [65] and [8]. \square

Algorithm 4.2. (Exact simulation of pre-jump intensity level for TS-contagion.) For the TS-contagion, conditional on the intensity level λ_{T_i} and the realisation of the $(i + 1)$ th interarrival time $\tau_{i+1} = \tau$, the distribution of the $(i + 1)$ th pre-jump intensity level $\lambda_{T_i+\tau^-}$ can be exactly decomposed by

$$\lambda_{T_i+\tau^-} | \lambda_{T_i} \stackrel{D}{=} w\lambda_{T_i} + \tilde{T}S + \tilde{B} \times S + \sum_{k=1}^{\tilde{N}} S_k, \tag{4.8}$$

where $\tilde{T}S$, \tilde{B} , S , \tilde{N} and $\{S_k\}_{k=1,2,\dots}$ are all independent of each other,

- $\tilde{T}S$ is an TS random variable of

$$\tilde{T}S \sim \text{TS}\left(\alpha, \frac{\kappa}{w} - \frac{1}{\delta}, \frac{\theta\rho}{\alpha\delta}(1 - w^\alpha)\right), \quad \kappa := \beta + \frac{1}{\delta}, \tag{4.9}$$

- \tilde{B} is a Bernoulli random variable taking 0 with probability p_1 and 1 with probability p_2 , and

$$p_1 := \frac{w\lambda_{T_i}}{(\theta\rho D/\delta)\Gamma(1 - \alpha) + w\lambda_{T_i}}, \quad p_2 := \frac{(\theta\rho D/\delta)\Gamma(1 - \alpha)}{(\theta\rho D/\delta)\Gamma(1 - \alpha) + w\lambda_{T_i}},$$

$$D := \frac{\delta}{\alpha} \left[\left(\kappa - \frac{w}{\delta}\right)^\alpha - \beta^\alpha \right],$$

- S is a mixture-gamma random variable of

$$S \sim \text{Gamma}\left(1 - \alpha, \kappa V_0 - \frac{1}{\delta}\right)$$

and

$$V_0 \stackrel{D}{=} \left[\delta\beta + 1 - \delta \left(\frac{\alpha D}{\delta} U_2 + \beta^\alpha\right)^{1/\alpha} \right]^{-1}, \quad U_2 \sim \mathbf{U}[0, 1], \tag{4.10}$$

- \tilde{N} is a Poisson random variable of rate

$$\frac{\theta\rho}{\alpha\delta} \kappa \Gamma(1 - \alpha) D_w$$

and

$$D_w := \int_1^{1/w} \frac{1 - u^{-\alpha}}{(\kappa u - 1/\delta)^{1-\alpha}} du,$$

- $\{S_k\}_{k=1,2,\dots}$ are i.i.d. with $S_k \sim \text{Gamma}(1 - \alpha, \kappa V - 1/\delta)$, and V can be exactly simulated via the A/R scheme of Algorithm C.1.

Proof. Algorithm (4.2) is another explicit specification of Theorem 3.2. Similarly to the previous gamma case in Algorithm 4.1, given the Lévy measure (4.3), we can identify that (3.11) is the Laplace transform of $\tilde{B} \times S$ from the calculation

$$\begin{aligned} & \frac{\rho}{\delta} \int_0^\infty e^{-vs} \int_s^{s/w} e^{s/\delta} e^{-y/\delta} \nu(dy) ds + w\lambda_{T_i} \\ & \frac{\rho}{\delta} \int_0^\infty \int_s^{s/w} e^{s/\delta} e^{-y/\delta} \nu(dy) ds + w\lambda_{T_i} \\ & = \frac{\theta\rho}{\delta} \int_0^\infty e^{-vs} \int_1^{1/w} s^{(1-\alpha)-1} e^{-(\kappa u - 1/\delta)s} u^{-1-\alpha} du ds + w\lambda_{T_i} \\ & = \frac{\int_0^\infty \int_1^{1/w} s^{(1-\alpha)-1} e^{-(\kappa u - 1/\delta)s} u^{-1-\alpha} du ds + w\lambda_{T_i}}{\int_0^\infty \int_1^{1/w} s^{(1-\alpha)-1} e^{-(\kappa u - 1/\delta)s} u^{-1-\alpha} du ds + w\lambda_{T_i}} \\ & = \frac{w\lambda_{T_i}}{(\theta\rho D/\delta)\Gamma(1-\alpha) + w\lambda_{T_i}} \times 1 + \frac{(\theta\rho D/\delta)\Gamma(1-\alpha)}{(\theta\rho D/\delta)\Gamma(1-\alpha) + w\lambda_{T_i}} \\ & \quad \times \int_0^\infty e^{-vs} \int_1^{1/w} \frac{(\kappa u - 1/\delta)^{1-\alpha}}{\Gamma(1-\alpha)} s^{(1-\alpha)-1} e^{-(\kappa u - 1/\delta)s} \frac{u^{-1-\alpha}}{D(\kappa u - 1/\delta)^{1-\alpha}} du ds \\ & = p_1 \times \mathbb{E}[e^{-v0}] + p_2 \times \mathbb{E}[e^{-vS}], \end{aligned}$$

where

$$D = \int_1^{1/w} \frac{u^{-1-\alpha}}{(\kappa u - 1/\delta)^{1-\alpha}} du = \frac{\delta}{\alpha} \left[\left(\kappa - \frac{w}{\delta} \right)^\alpha - \beta^\alpha \right].$$

Hence, the outcome of $\tilde{B} \times S$ is trivially equal to 0 with probability p_1 or the random variable S with probability p_2 . S follows a mixture-gamma distribution with shape parameter $1 - \alpha$ and rate parameter $\kappa V_0 - 1/\delta$. Here, V_0 is a well-defined random variable with density function

$$f_{V_0}(u) = \frac{u^{-\alpha-1}}{D(\kappa u - 1/\delta)^{1-\alpha}}, \quad u \in \left[1, \frac{1}{w} \right].$$

It can be directly simulated via the explicit inverse transform (4.10), as its CDF is

$$F_{V_0}(u) = \frac{\delta}{\alpha D} \left[u^{-\alpha} \left(\kappa u - \frac{1}{\delta} \right)^\alpha - \beta^\alpha \right], \quad u \in \left[1, \frac{1}{w} \right].$$

The first two terms of (3.8), i.e. (3.12), can be expressed by

$$\begin{aligned} & \frac{\mathbb{E}[e^{-v\lambda_{T_i+\tau^-}} e^{-(\Lambda_{T_i+\tau^-} - \Lambda_{T_i})} | \lambda_{T_i}]}{\mathbb{E}[e^{-(\Lambda_{T_i+\tau^-} - \Lambda_{T_i})} | \lambda_{T_i}]} \\ & = e^{-vw\lambda_{T_i}} \times \exp \left(-\frac{\theta\rho}{\alpha\delta} (1-w^\alpha) \int_0^\infty (1-e^{-vs}) \frac{1}{s^{\alpha+1}} e^{-(\kappa/w-1/\delta)s} ds \right) \\ & \quad \times \exp \left(-\frac{\theta\rho}{\alpha\delta} \kappa \Gamma(1-\alpha) I \right), \end{aligned}$$

where

$$I = \int_0^\infty (1-e^{-vs}) \int_1^{1/w} \frac{(\kappa u - 1/\delta)^{1-\alpha}}{\Gamma(1-\alpha)} s^{(1-\alpha)-1} \frac{1-u^{-\alpha}}{(\kappa u - 1/\delta)^{1-\alpha}} du ds,$$

since the Lévy measure ν for the TS subordinator is specified in (4.3), and the Laplace exponent of (3.12) can be rewritten as

$$\begin{aligned} & \rho \int_{\nu}^{1/\delta+(v-1/\delta)w} \frac{\Phi(u - \frac{u-1/\delta}{v-1/\delta}v) - \Phi(u)}{1 - \delta u} du \\ &= \frac{\rho}{\delta} \int_0^\infty (1 - e^{-vs}) \frac{1}{s} e^{s/\delta} \int_s^{s/w} \frac{\theta}{y^{\alpha+1}} e^{-\kappa s/w} dy ds \\ & \quad + \frac{\rho}{\delta} \int_0^\infty (1 - e^{-vs}) \frac{e^{s/\delta}}{s} \int_s^{s/w} \frac{\theta(e^{-\kappa y} - e^{-\kappa s/w})}{y^{\alpha+1}} dy ds \\ &= \int_0^\infty (1 - e^{-vs}) \frac{\theta\rho}{\alpha\delta} (1 - w^\alpha) \frac{1}{s^{\alpha+1}} e^{-(\kappa/w-1/\delta)s} ds \\ & \quad + \frac{\theta\rho}{\alpha\delta} \kappa \Gamma(1 - \alpha) J \end{aligned}$$

where

$$J = \int_0^\infty (1 - e^{-vs}) \int_1^{1/w} \frac{(\kappa u - 1/\delta)^{1-\alpha}}{\Gamma(1 - \alpha)} s^{(1-\alpha)-1} e^{-(\kappa u-1/\delta)s} \frac{1 - u^{-\alpha}}{(\kappa u - 1/\delta)^{1-\alpha}} du ds.$$

So, for (3.12), it consists of three components: one deterministic trend, a TS process, and a compound Poisson process. In particular, the rate of the compound Poisson process is \tilde{N} is

$$\frac{\theta\rho}{\alpha\delta} \kappa \Gamma(1 - \alpha) D_w,$$

and the jump sizes follow a mixture-gamma distribution with shape parameter $(1 - \alpha)$ and rate parameter $\kappa V - 1/\delta$. Here, V is a well-defined random variable with density

$$f_V(u) = \frac{1 - u^{-\alpha}}{D_w(\kappa u - 1/\delta)^{1-\alpha}}, \quad u \in \left[1, \frac{1}{w}\right]. \tag{4.11}$$

Overall, we have the conditional Laplace transform of pre-jump intensity level explicitly as

$$\begin{aligned} & \mathbb{E}\left[e^{-v\lambda_{T_i+\tau_{i+1}^-} | \tau_{i+1} = \tau, \lambda_{T_i}}\right] \\ &= e^{-vw\lambda_{T_i}} \times \exp\left(-\frac{\theta\rho}{\alpha\delta} (1 - w^\alpha) \int_0^\infty (1 - e^{-vs}) \frac{1}{s^{\alpha+1}} e^{-(\kappa/w-1/\delta)s} ds\right) \\ & \quad \times \exp\left(-\frac{\theta\rho}{\alpha\delta} \kappa \Gamma(1 - \alpha) D_w K\right) \\ & \quad \times \left[\frac{w\lambda_{T_i}}{(\theta\rho D/\delta)\Gamma(1 - \alpha) + w\lambda_{T_i}} + \frac{(\theta\rho D/\delta)\Gamma(1 - \alpha)}{(\theta\rho D/\delta)\Gamma(1 - \alpha) + w\lambda_{T_i}} \right. \\ & \quad \left. \times \int_0^\infty e^{-vs} \int_1^{1/w} \frac{(\kappa u - 1/\delta)^{1-\alpha}}{\Gamma(1 - \alpha)} s^{(1-\alpha)-1} e^{-(\kappa u-1/\delta)s} \frac{u^{-1-\alpha}}{D(\kappa u - 1/\delta)^{1-\alpha}} du ds \right], \end{aligned}$$

where

$$K = \int_0^\infty (1 - e^{-vs}) \int_1^{1/w} \frac{(\kappa u - 1/\delta)^{1-\alpha}}{\Gamma(1 - \alpha)} s^{(1-\alpha)-1} \frac{1 - u^{-\alpha}}{D_w(\kappa u - 1/\delta)^{1-\alpha}} du ds.$$

We can identify from the Laplace transforms above that the distribution of the $(i + 1)$ th pre-jump intensity level $\lambda_{T_i+\tau^-}$ conditional on λ_{T_i} is exactly equal in distribution to the sum of four simple elements provided in (4.8). All these components can be simulated exactly. To simulate the TS random variable, one could use existing algorithms provided in [23], [53], [73] or backward recursive (BR) scheme provided in [50]. And to sample the compound Poisson random variable \tilde{N} , one first needs to generate the intermediate random variable V with density (4.11). Since there is no closed form for the inverse function of the CDF of V , we have to rely on the A/R scheme of Algorithm C.1. \square

Exact simulation of self-exciting jumps. Conditional on the realisations of the interarrival time and pre-jump intensity level as above, the associated self-exciting jump can easily be simulated by just following Algorithm 3.3 in general both for gamma and TS contagion processes.

5. Numerical experiments

In this section, let us take the TS-contagion model as an example to illustrate the performance of our exact scheme via extensive numerical experiments, and postpone the implementation of the gamma-contagion model to Section 6 with more financial applications. The simulation experiments here and elsewhere in this paper are all conducted on a desktop PC with an Intel® Core™ i7-3770S CPU@3.10 GHz processor, 8.00 GB RAM, Windows 7®, 64-bit Operating System; the algorithms are coded and performed in MATLAB® (R2014a), and the computation time is measured by the *elapsed CPU time* in seconds. The true value of the conditional expectation of N_T for any fixed time $T > 0$ provided in Proposition 2.1 is used to numerically validate and test our algorithms. The associated errors from the true values are reported by three standard measures.

(i) *Error* = estimated value – true value.

(ii) *Relative error (error %)* = $\frac{\text{estimated value} - \text{true value}}{\text{true value}}$.

(iii) *Root mean square error RMSE* = $\sqrt{\text{bias}^2 + \text{SE}^2}$, where the SE is the standard error of simulation output, and the bias is the difference between the expectation of the estimator and the associated true (theoretical) value. For the algorithm of exact simulation here, the bias is conventionally set to zero.

We implement Algorithm 3.3 for the TS and IG cases in a fixed period of $[0, T]$ with and without self-exciting jumps.

Case I. *Jump process with non-Gaussian OU intensity* (see Definition 2.1).

Case II. *Self-exciting jump process with non-Gaussian OU intensity* (of Definition 2.2).

Note that as an intermediate step we have to generate the random variable \tilde{TS} of (4.9) in Algorithm 4.2 for the general TS case. Several algorithms are available in the literature, including approximation-based algorithms such as *infinite series representation* [91] and exact algorithms such as *simple stable rejection* (SSR) [23], the *double rejection algorithm* [53], the *fast rejection algorithm* [73], and the *backward recursive (BR) scheme* [50]. However, the choice of algorithms is in fact not the focus of our paper. For the purpose of demonstration, we adopt the BR scheme. It works extremely efficiently for some families, including those

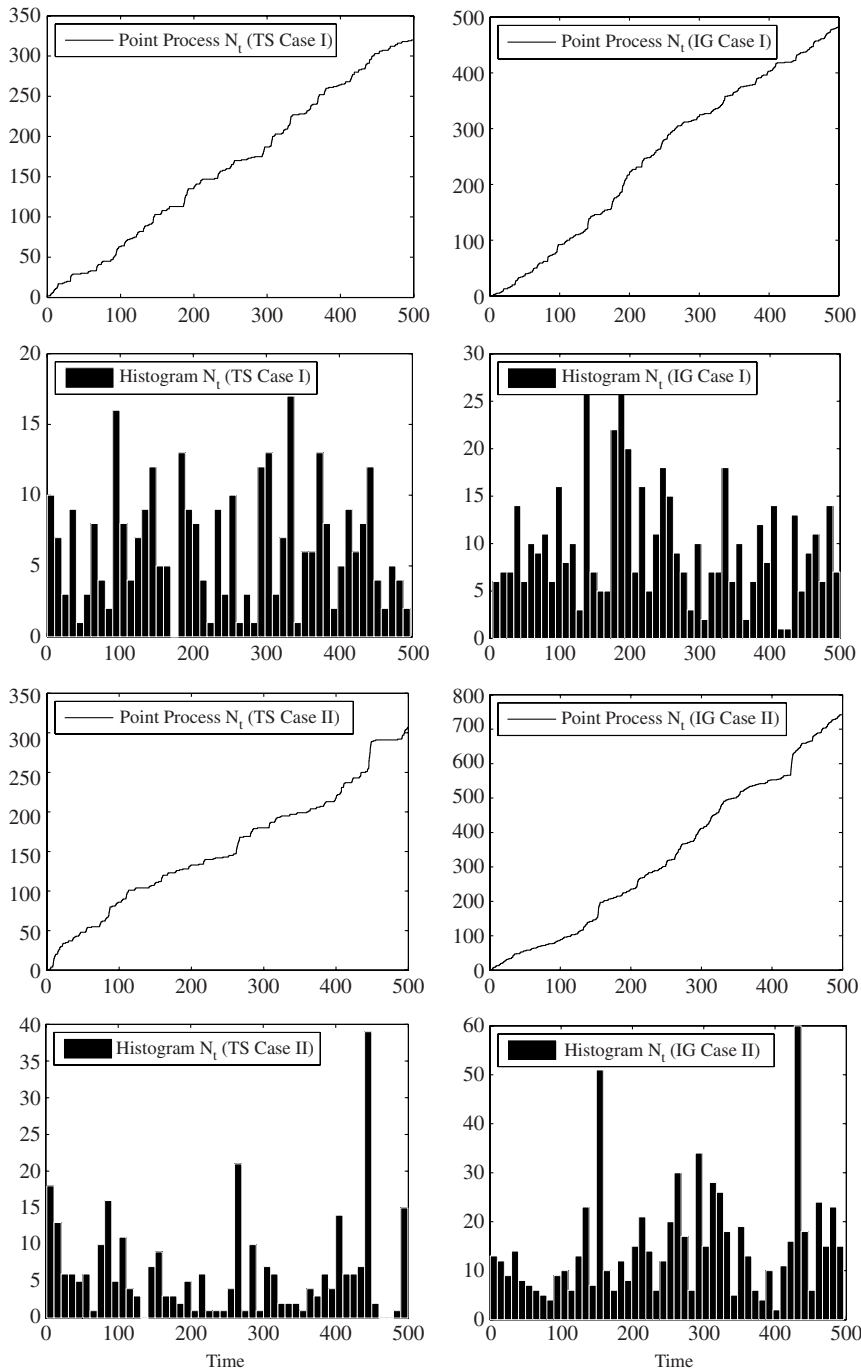


FIGURE 3: Simulated sample paths of the point processes and the associated time-series plots for Cases I and II: TS Case I $(\delta, \rho; \alpha, \beta, \theta; \lambda_0) = (1.0, 0.5; 0.25, 0.2, 0.25; 0.5)$, TS Case II $(\delta, \rho; \alpha, \beta, \theta; \gamma; \lambda_0) = (1.0, 0.5; 0.25, 0.2, 0.25; 5.0; 0.5)$; IG Case I $(\delta, \rho; c; \lambda_0) = (1.0, 0.5; 0.5; 0.5)$, IG Case II $(\delta, \rho; c; \gamma; \lambda_0) = (1.0, 0.5; 0.5; 4.0; 0.5)$.

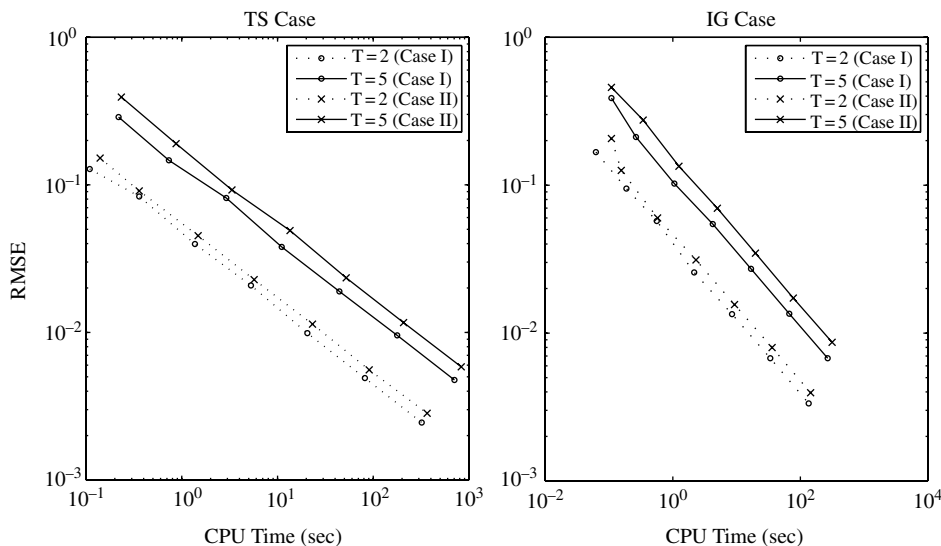


FIGURE 4: Convergence analysis via RMSE versus CPU time by log-log plots for Cases I and II: TS Case I $(\delta, \rho; \alpha, \beta, \theta; \lambda_0) = (1.0, 0.5; 0.25, 0.2, 0.25; 0.5)$, TS Case II $(\delta, \rho; \alpha, \beta, \theta; \gamma; \lambda_0) = (1.0, 0.5; 0.25, 0.2, 0.25; 5.0; 0.5)$; IG Case I $(\delta, \rho; c; \lambda_0) = (1.0, 0.5; 0.5; 0.5)$, IG Case II $(\delta, \rho; c; \gamma; \lambda_0) = (1.0, 0.5; 0.5; 4.0; 0.5)$.

with stability index the *binary fractions* $1/2^n$, $n = 1, 2, \dots$, which can easily be simulated by recursively generating IG random variables without the A/R mechanism. For a general parameter setting, one could simply adopt other algorithms such as the SSR scheme of Algorithm E.1.

For numerical implementation, we further assume that the sizes of self-exciting jumps follow an exponential distribution of rate $\gamma > 0$, i.e. $X_i \sim \text{Exp}(\gamma)$, and the stable index takes the values of, say, $\alpha = 1/4$ for the TS case and $\alpha = 1/2$ for the IG case, respectively. $\tilde{T}S$ of (4.9) is simulated using the BR scheme specifically designed for $\alpha = 1/4$ in Algorithm D.1, and the parameters are set as follows.

TS Case I. $(\delta, \rho; \alpha, \beta, \theta; \lambda_0) = (1.0, 0.5; 0.25, 0.2, 0.25; 0.5)$.

TS Case II. $(\delta, \rho; \alpha, \beta, \theta; \gamma; \lambda_0) = (1.0, 0.5; 0.25, 0.2, 0.25; 5.0; 0.5)$.

IG Case I. $(\delta, \rho; c; \lambda_0) = (1.0, 0.5; 0.5; 0.5)$.

IG Case II. $(\delta, \rho; c; \gamma; \lambda_0) = (1.0, 0.5; 0.5; 4.0; 0.5)$.

Simulated sample paths of the point processes within a long period of $t \in [0, 500]$ with the associated histograms are plotted in Figure 3, where the clustering or ‘contagious’ arrivals of jumps can be clearly presented. Furthermore, to measure the accuracy and efficiency of our scheme, we carry out the convergence analysis: Figure 4 presents log-log plots for the RMSE against the CPU time for each case in two different time horizons $T = 2, 5$, respectively, and the associated results in detail are reported in Tables 1 and 2. Overall, from the numerical results reported in this section, it is evident that our exact scheme can achieve a very high level of accuracy and efficiency.

TABLE 1: Simulation results for Cases I and II: TS Case I $(\delta, \rho; \alpha, \beta, \theta; \lambda_0) = (1.0, 0.5; 0.25, 0.2, 0.25; 0.5)$, TS Case II $(\delta, \rho; \alpha, \beta, \theta; \gamma; \lambda_0) = (1.0, 0.5; 0.25, 0.2, 0.25; 5.0; 0.5)$.

| Case | Paths | True | Simulation | Error | Error% | RMSE | CPU time (sec) |
|------------------|---------|--------|------------|---------|----------|--------|----------------|
| TS case | | | | | | | |
| Case I, $T = 2$ | 100 | 1.0138 | 0.9300 | -0.0838 | -8.2683% | 0.1281 | 0.11 |
| | 400 | 1.0138 | 1.0525 | 0.0387 | 3.8146% | 0.0834 | 0.36 |
| | 1 600 | 1.0138 | 1.0363 | 0.0224 | 2.2118% | 0.0398 | 1.37 |
| | 6 400 | 1.0138 | 1.0184 | 0.0046 | 0.4548% | 0.0208 | 5.29 |
| | 25 600 | 1.0138 | 1.0167 | 0.0029 | 0.2853% | 0.0099 | 20.53 |
| | 102 400 | 1.0138 | 1.0133 | -0.0005 | -0.0509% | 0.0049 | 81.74 |
| | 409 600 | 1.0138 | 1.0127 | -0.0012 | -0.1147% | 0.0024 | 321.78 |
| Case I, $T = 5$ | 100 | 2.5488 | 2.5500 | 0.0012 | 0.0472% | 0.2879 | 0.22 |
| | 400 | 2.5488 | 2.4700 | -0.0788 | -3.0915% | 0.1466 | 0.73 |
| | 1 600 | 2.5488 | 2.6413 | 0.0925 | 3.6274% | 0.0815 | 2.92 |
| | 6 400 | 2.5488 | 2.5308 | -0.0180 | -0.7068% | 0.0380 | 11.08 |
| | 25 600 | 2.5488 | 2.5523 | 0.0035 | 0.1361% | 0.0190 | 44.29 |
| | 102 400 | 2.5488 | 2.5589 | 0.0101 | 0.3948% | 0.0095 | 177.92 |
| | 409 600 | 2.5488 | 2.5437 | -0.0051 | -0.1998% | 0.0048 | 706.82 |
| Case II, $T = 2$ | 100 | 1.1406 | 1.1500 | 0.0094 | 0.8281% | 0.1520 | 0.14 |
| | 400 | 1.1406 | 1.0925 | -0.0481 | -4.2133% | 0.0909 | 0.36 |
| | 1 600 | 1.1406 | 1.1581 | 0.0176 | 1.5404% | 0.0453 | 1.48 |
| | 6 400 | 1.1406 | 1.1233 | -0.0173 | -1.5145% | 0.0228 | 5.71 |
| | 25 600 | 1.1406 | 1.1468 | 0.0062 | 0.5472% | 0.0114 | 23.21 |
| | 102 400 | 1.1406 | 1.1305 | -0.0101 | -0.8835% | 0.0056 | 90.92 |
| | 409 600 | 1.1406 | 1.1454 | 0.0049 | 0.4282% | 0.0028 | 365.82 |
| Case II, $T = 5$ | 100 | 3.0290 | 2.9900 | -0.0390 | -1.2891% | 0.3932 | 0.23 |
| | 400 | 3.0290 | 3.0875 | 0.0585 | 1.9298% | 0.1903 | 0.87 |
| | 1 600 | 3.0290 | 3.0413 | 0.0122 | 0.4029% | 0.0923 | 3.34 |
| | 6 400 | 3.0290 | 3.0961 | 0.0670 | 2.2135% | 0.0491 | 13.54 |
| | 25 600 | 3.0290 | 3.0095 | -0.0196 | -0.6456% | 0.0234 | 52.28 |
| | 102 400 | 3.0290 | 3.0264 | -0.0026 | -0.0862% | 0.0117 | 207.73 |
| | 409 600 | 3.0290 | 3.0308 | 0.0017 | 0.0569% | 0.0058 | 831.64 |

To be even more prudent, the simulation for the interarrival time based on the *simplified thinning scheme* of Algorithm 3.2, as an intermediate step, can also be tested separately. To numerically assess its accuracy and efficiency, we compare the simulated results of V^* with its theoretical tail distribution $\mathbb{P}\{V^* > \tau\}$ as specified in (3.6), which can be calculated explicitly by substituting the Laplace exponent Φ from (4.4). We set the parameters by $(\delta, \rho; \alpha, \beta, \theta) = (0.5, 1.0; 0.9, 0.2, 0.25)$, and each estimation is based on 10^5 replications. Error percentages (*Error%*) for measuring *relative errors* are reported in Table 3. The total CPU time for producing the whole Table 3 is only 12.64 seconds, and the error percentages are all very tiny.

TABLE 2: Simulation results for Cases I and II: IG Case I $(\delta, \rho; c; \lambda_0) = (1.0, 0.5; 0.5; 0.5)$, IG Case II $(\delta, \rho; c; \gamma; \lambda_0) = (1.0, 0.5; 0.5; 4.0; 0.5)$.

| Case | Paths | True | Simulation | Error | Error% | RMSE | CPU time (sec) |
|------------------|---------|--------|------------|---------|----------|--------|----------------|
| Case I, $T = 2$ | 100 | 1.5677 | 1.5000 | -0.0677 | -4.3165% | 0.1673 | 0.06 |
| | 400 | 1.5677 | 1.6025 | 0.0348 | 2.2219% | 0.0948 | 0.19 |
| | 1 600 | 1.5677 | 1.6431 | 0.0755 | 4.8134% | 0.0573 | 0.56 |
| | 6 400 | 1.5677 | 1.5311 | -0.0366 | -2.3330% | 0.0257 | 2.17 |
| | 25 600 | 1.5677 | 1.5745 | 0.0068 | 0.4328% | 0.0134 | 8.50 |
| | 102 400 | 1.5677 | 1.5743 | 0.0066 | 0.4229% | 0.0068 | 33.77 |
| | 409 600 | 1.5677 | 1.5687 | 0.0011 | 0.0673% | 0.0033 | 135.05 |
| Case I, $T = 5$ | 100 | 4.5034 | 4.1500 | -0.3534 | -7.8468% | 0.3880 | 0.11 |
| | 400 | 4.5034 | 4.3075 | -0.1959 | -4.3494% | 0.2118 | 0.27 |
| | 1 600 | 4.5034 | 4.3394 | -0.1640 | -3.6416% | 0.1026 | 1.06 |
| | 6 400 | 4.5034 | 4.5084 | 0.0051 | 0.1125% | 0.0546 | 4.23 |
| | 25 600 | 4.5034 | 4.5268 | 0.0234 | 0.5202% | 0.0272 | 16.83 |
| | 102 400 | 4.5034 | 4.5236 | 0.0203 | 0.4500% | 0.0135 | 67.08 |
| | 409 600 | 4.5034 | 4.5037 | 0.0003 | 0.0067% | 0.0068 | 268.24 |
| Case II, $T = 2$ | 100 | 1.8035 | 1.7100 | -0.0935 | -5.1832% | 0.21 | 0.11 |
| | 400 | 1.8035 | 1.7925 | -0.0110 | -0.6087% | 0.13 | 0.16 |
| | 1 600 | 1.8035 | 1.7644 | -0.0391 | -2.1682% | 0.06 | 0.58 |
| | 6 400 | 1.8035 | 1.7758 | -0.0277 | -1.5357% | 0.03 | 2.31 |
| | 25 600 | 1.8035 | 1.8043 | 0.0008 | 0.0454% | 0.02 | 9.31 |
| | 102 400 | 1.8035 | 1.8025 | -0.0010 | -0.0569% | 0.01 | 36.07 |
| | 409 600 | 1.8035 | 1.8039 | 0.0004 | 0.0232% | 0.00 | 145.36 |
| Case II, $T = 5$ | 100 | 5.5817 | 5.2400 | -0.3417 | -6.1216% | 0.4584 | 0.11 |
| | 400 | 5.5817 | 5.4000 | -0.1817 | -3.2550% | 0.2753 | 0.34 |
| | 1 600 | 5.5817 | 5.6300 | 0.0483 | 0.8656% | 0.1344 | 1.25 |
| | 6 400 | 5.5817 | 5.5902 | 0.0085 | 0.1517% | 0.0698 | 4.99 |
| | 25 600 | 5.5817 | 5.5648 | -0.0169 | -0.3024% | 0.0347 | 19.83 |
| | 102 400 | 5.5817 | 5.5777 | -0.0040 | -0.0713% | 0.0173 | 77.70 |
| | 409 600 | 5.5817 | 5.5738 | -0.0079 | -0.1419% | 0.0087 | 315.71 |

TABLE 3: Comparison between the theoretical formulas and the associated simulation results for the *simplified thinning scheme* of Algorithm 3.2 with each estimation based on 10^5 replications.

| τ | $\mathbb{P}\{V^* > \tau\}$ | Simulation | Error% |
|--------|----------------------------|------------|----------|
| 0.1 | 98.66% | 98.62% | -0.0367% |
| 0.2 | 94.87% | 94.80% | -0.0752% |
| 0.3 | 89.10% | 89.01% | -0.0965% |
| 0.4 | 81.85% | 81.81% | -0.0499% |
| 0.5 | 73.66% | 73.60% | -0.0819% |
| 0.6 | 65.01% | 64.86% | -0.2268% |
| 0.7 | 56.35% | 56.12% | -0.3943% |
| 0.8 | 48.00% | 47.89% | -0.2333% |
| 0.9 | 40.24% | 40.15% | -0.2239% |
| 1.0 | 33.22% | 33.13% | -0.2773% |

6. Comprehensive risk analysis for a large portfolio facing contagious losses and unexpected exogenous gamma shocks

It has now been widely recognised among academics and financial practitioners that risk spreads through highly interconnected business networks, and defaults could trigger more defaults via a ‘domino’ effect. The resulting losses presented in financial markets could be amplified. As earlier mentioned in Section 4, gamma distribution is a popular building block in financial applications. In particular, it plays an important role in credit risk modelling. For instance, both the widely used framework of [42] in the banking industry and influential papers by [67], [68], and [59] in the literature, assumed that macroeconomic factors are driven by independent gamma-distributed random variables. Further, it can also be equipped as a fundamental risk driver for price movements, e.g. the popular *variance gamma model* [83, 84]. More recent evidence has been found by [64] that long periods with relatively few defaults are followed by episodes of significant clustering of defaults, and the resulting distribution of default rates is highly skewed towards large values. This motivates us to adopt our new model of gamma contagion as an example for applications in risk management for a portfolio facing a ‘domino’ effect of losses. We assume that exogenous commonly shared risk is dynamically powered by a gamma process. More precisely, we adopt the gamma distribution as the fundamental driver of randomness (or *gamma shock*) to construct the *OU- Γ interarrival intensity* for a point process N_t in Definition 2.2. A simulated path of this interarrival intensity process within the time period $t \in [0, 5]$ based on the parameter setting $(\delta, \rho; a, b; \lambda_0) = (1.0, 1.0; 4.0, 0.5; 2.0)$ was plotted in Figure 1 above, where we can observe relatively high-frequency and small shocks. In fact, Barndorff-Nielsen and Shephard [17] called it the *OU- Γ process*, and it has become a very popular tool for modelling stochastic volatilities in a continuous-time set-up. Hainaut and Devolder [69] used it as a special case of Cox processes to model human mortality rates, and applied to actuarial valuation in insurance. Eberlein, Madan, Pistorius, and Yor [57] treated it as a one-factor model for describing the evolution of instantaneous interest rates.

In reality, contagion may be triggered by losses or defaults of banks or other financial institutions through inter-institutional lendings in the interbank market, or it may be further amplified due to some common asset holdings of overlapping portfolios [27]. We offer some numerical examples of comprehensive risk analysis for a large portfolio facing contagious defaults and losses. We construct a simple contagious loss process to capture the propagated defaults for a generic large pool of financial institutions (banks for short) within a financial system. The following framework, of course, would work generically for other similar institutions. The *aggregate loss process* of this large portfolio by time t is

$$L_t = \sum_{i=1}^{N_t} L_i, \quad t \geq 0,$$

where N_t is a Γ -contagion process, and $L_i \geq 0$ is the absolute value of the loss size for the i th default, of which the mean is denoted by $\mu_L := \mathbb{E}[L_i]$ for any index i . We assume that the sizes of self-exciting jumps in (2.3) generally satisfy

$$X_i = \varpi_i \times g(H_i), \quad (6.1)$$

where

- H_i is the history of the loss path until time t , i.e. $H_i := \{L_j\}_{j < i} \cup \{T_j\}_{j \leq i}$,
- $\varpi_i > 0$ is the *amplification multiplier*, the amplification mechanisms during financial crises in detail were described and analysed in [25], [26], and more recently in [2], which

might be dependent on the degree of *financial connectivity* of the underlying company i to others, or the effects of policymakers' interventions to limit the extent of contagion,

- $g(\cdot)$ is a general non-negative function of the losses. Since the jump sizes in (6.1) follow a $\mathcal{F}_{T_i^-}$ -measurable distribution as explained earlier in Definition 2.2, similarly the function $g(\cdot)$ is also very general, and it can include all past losses, that is,

$$g(\cdot) = g(T_1, T_2, \dots, T_i, L_1, \dots, L_{i-1}),$$

which could adopt functional forms, for example, assigning weight to each loss size according to its loss time or similarly to autoregressive time series models.

In fact, (6.1) provides a channel for contagion (or feedback) effects of market participants' reactions to adverse scenarios. The economic interpretation for this model is that the impacts and the timing of unexpected *exogenous gamma shocks* acting on the entire portfolio as macroeconomic scenarios are modelled by a mean-reverting gamma-driven OU process. The shocks might not lead to an immediate default but act on the underlying intensity via a positive jump, which increases the default probability afterwards. Meanwhile, *endogenic shocks*, i.e. contagious losses due to the propagated defaults, are modelled by self-exciting jumps, and the associated magnitudes can be captured by jump sizes $\{X_i\}_{i=1,2,\dots}$.

The great flexibility of our exact simulation scheme allows us to accurately and efficiently generate highly comprehensive scenarios for risk assessment. In general, our algorithms can simulate sample paths when loss sizes L_i may depend on the entire history of N_t and λ_t before or at time T_i . We discuss several circumstances that can be captured by our models as follows.

6.1. A simple benchmark model

The loss occurring within a financial institution may spread via various business channels and eventually trigger subsequent losses of others in markets. Intuitively, a larger loss may make a larger impact. For convenience of illustration, we assume that the sizes of self-exciting jumps satisfy

$$X_i = \bar{\omega} \times L_i,$$

where $\bar{\omega} > 0$ is the *average amplification multiplier*, meaning that each investment has a linear and homogeneous amplification effect. We further assume that each loss size is exponentially distributed, i.e. $L_i \sim \text{Exp}(\ell)$, $\ell > 0$ with mean $\mu_L := 1/\ell$. To assess the overall risk of this portfolio, we implement the exact simulation of Algorithms 3.3 and 4.1 with (Case I) and without (Case II) contagion in the fixed time period $[0, t]$, respectively:

Case I. $(\delta, \rho; a, b; \lambda_0) = (0.5, 0.5; 0.5, 2.0; 0.5)$,

Case II. $(\delta, \rho; a, b; \ell, \bar{\omega}; \lambda_0) = (0.5, 0.5; 0.5, 2.0; 8.0, 2.0; 0.5)$.

We concentrate on the default number N_t in the system. Case I or II can be considered as a benchmark model, as by Proposition 2.1 the expected default number has analytical forms.

Proposition 6.1. (Expectation of N_t .) *The expected default number until time t is given by*

$$\mathbb{E}[N_t | \lambda_0] = \lambda_0 \frac{1 - e^{-\eta t}}{\eta} + \frac{\rho}{\eta} \left(t - \frac{1 - e^{-\eta t}}{\eta} \right) \frac{a}{b}, \quad \eta \neq 0, \tag{6.2}$$

where

$$\eta = \begin{cases} \delta & \text{for Case I,} \\ \delta - \bar{\omega}/\ell & \text{for Case II.} \end{cases}$$

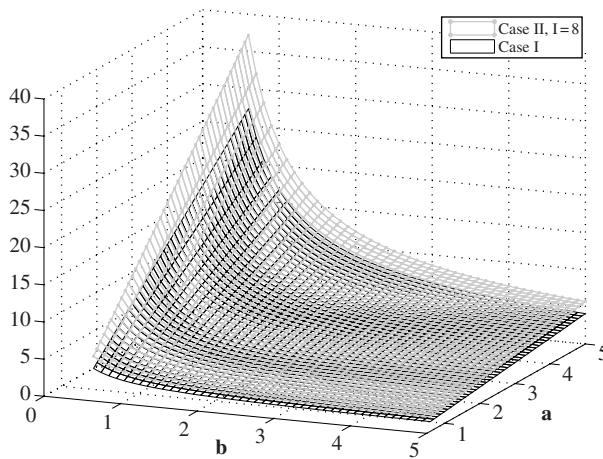


FIGURE 5: Sensitivity analysis for the expected number of defaults $\mathbb{E}[N_{t=5} | \lambda_0]$ with respect to a and b based on the parameters $(\delta, \rho; \bar{\omega}; \lambda_0) = (0.5, 0.5; 2.0; 0.5)$.

TABLE 4: Simulation results for Cases I and II and time $t = 2, 5$: $(\delta, \rho; a, b; \lambda_0) = (0.5, 0.5; 0.5, 2.0; 0.5)$ for Case I, and $(\delta, \rho; a, b; \ell, \bar{\omega}; \lambda_0) = (0.5, 0.5; 0.5, 2.0; 8.0, 2.0; 0.5)$ for Case II.

| Case | Paths | True | Simulation | Error | Error% | RMSE | CPU time (sec) |
|------------------|-----------|--------|------------|---------|--------|--------|----------------|
| Case I, $t = 2$ | 10 000 | 0.8161 | 0.8154 | -0.0007 | -0.08% | 0.0094 | 5.00 |
| | 40 000 | 0.8161 | 0.8151 | -0.0010 | -0.12% | 0.0047 | 19.50 |
| | 160 000 | 0.8161 | 0.8135 | -0.0026 | -0.31% | 0.0024 | 80.13 |
| | 640 000 | 0.8161 | 0.8159 | -0.0001 | -0.02% | 0.0012 | 322.89 |
| | 2 560 000 | 0.8161 | 0.8163 | 0.0003 | 0.03% | 0.0006 | 1 280.63 |
| Case I, $t = 5$ | 10 000 | 1.7090 | 1.7297 | 0.0207 | 1.21% | 0.0152 | 9.66 |
| | 40 000 | 1.7090 | 1.6993 | -0.0097 | -0.57% | 0.0076 | 37.45 |
| | 160 000 | 1.7090 | 1.7085 | -0.0004 | -0.02% | 0.0038 | 148.38 |
| | 640 000 | 1.7090 | 1.7079 | -0.0010 | -0.06% | 0.0019 | 575.55 |
| | 2 560 000 | 1.7090 | 1.7083 | -0.0006 | -0.04% | 0.0009 | 2 291.14 |
| Case II, $t = 2$ | 10 000 | 1.0000 | 0.9983 | -0.0017 | -0.17% | 0.0128 | 5.94 |
| | 40 000 | 1.0000 | 1.0054 | 0.0054 | 0.54% | 0.0065 | 23.13 |
| | 160 000 | 1.0000 | 1.0073 | 0.0073 | 0.73% | 0.0032 | 92.63 |
| | 640 000 | 1.0000 | 1.0000 | 0.0000 | 0.00% | 0.0016 | 371.98 |
| | 2 560 000 | 1.0000 | 0.9995 | -0.0005 | -0.05% | 0.0008 | 1 489.06 |
| Case II, $t = 5$ | 10 000 | 2.5000 | 2.5060 | 0.0060 | 0.24% | 0.0263 | 13.06 |
| | 40 000 | 2.5000 | 2.4964 | -0.0036 | -0.14% | 0.0132 | 52.00 |
| | 160 000 | 2.5000 | 2.4882 | -0.0118 | -0.47% | 0.0065 | 201.44 |
| | 640 000 | 2.5000 | 2.4972 | -0.0028 | -0.11% | 0.0033 | 800.75 |
| | 2 560 000 | 2.5000 | 2.4983 | -0.0017 | -0.07% | 0.0016 | 3 197.61 |

To explore the models, let us first carry out a sensitivity analysis for the expected default number $\mathbb{E}[N_t | \lambda_0]$ with respect to their key parameters for controlling the external gamma shocks, a and b , with and without contagion, and the results are provided respectively in Figure 5. Numerical tests for our algorithms are based on the true means (6.2). The associated errors reported by three standard measures are reported in Table 4. Convergence analysis via

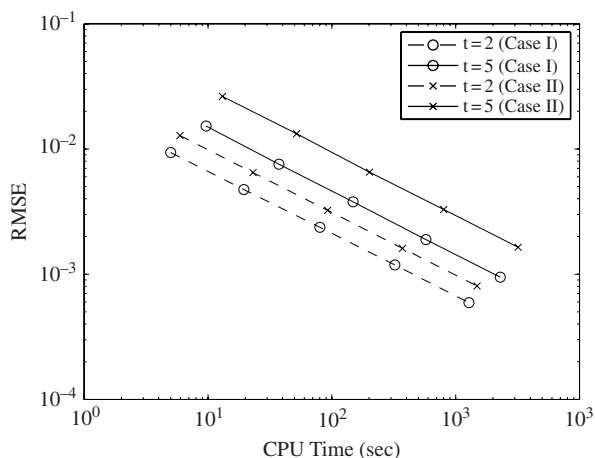


FIGURE 6: Convergence analysis via the log-log plots of the RMSE versus the CPU time for Cases I and II and $t = 2, 5$: $(\delta, \rho; a, b; \lambda_0) = (0.5, 0.5; 0.5, 2.0; 0.5)$ for Case I, and $(\delta, \rho; a, b; \ell, \bar{\omega}; \lambda_0) = (0.5, 0.5; 0.5, 2.0; 8.0, 2.0; 0.5)$ for Case II.

log-log plots of the RMSE against the CPU time for Cases I and II and $t = 2, 5$ is presented in Figure 6. We can observe that simulations are pretty fast with very tiny errors, which provides numerical evidence of accuracy and efficiency for our algorithms.

6.2. A model with contagion threshold

In reality, each loss might not necessarily cause contagion immediately throughout the entire system. Contagion may be only triggered when the loss exceeds a certain high level, that is, contagion is likely to occur only in severe scenarios, which has also been reported in [59]. This circumstance could be modelled by a mixture of Cases I and II, by assuming that the sizes of self-exciting jumps X_i satisfy

$$X_i = \omega_i \times (L_i - K_i)^+,$$

where $K_i \geq 0$ is the *contagion threshold* (i.e. the threshold that triggers the contagion effect of the i th loss L_i), and the contagion has been partially capped. If a bank is more vulnerable, its threshold is more easily reached. Alternatively, we may interpret K_i as a capital buffer, and it could be a certain quantile of the loss distribution L_i . If we assign the same quantile to all banks, it is equivalent to an identical economic capital applying to all banks, which is the assumption made by [59]. If the magnitude of loss overshoots the threshold, the bank may become insolvent, and this risk may then spread to other banks (through the interbank market) resulting in an increase in the default intensity of the entire system (but this would not immediately cause other defaults). If the thresholds are very high compared to the levels of loss, then it corresponds to a ‘weak contagion’ environment, whereas if the thresholds are very low, then it is a ‘strong contagion’ environment.

With the contagion threshold, contagion could be partially or fully triggered. Here, for numerical illustration, we assume that losses are exponentially distributed and the amplification multipliers and contagion thresholds are homogeneous, i.e. $L_i \sim \text{Exp}(\ell)$, $a_i \equiv \bar{\omega}$, and $K_i \equiv K \geq 0$. The expected default number can hardly capture the full picture of the risk, and we have to look at the entire distribution. We choose $K = \infty, 1/8, 0$ and plot the estimated probability mass function (PMF) of the total default number within the period of

TABLE 5: Quantiles of the default number $N_{t=5}$, estimated from 10^6 replications based on the parameter setting $(\delta, \rho; a, b; \ell, \bar{w}; \lambda_0) = (0.5, 0.5; 0.5, 2.0; 8.0, 2.0; 0.5)$, with homogeneous contagion thresholds $K = \infty, 1/8, 0$, respectively.

| K | Quantile | | | | | Mean | Min | Max |
|----------|----------|-----|-----|-----|-----|--------|-----|-----|
| | 5% | 25% | 50% | 75% | 95% | | | |
| ∞ | 0 | 1 | 1 | 2 | 5 | 1.7075 | 0 | 17 |
| 1/8 | 0 | 1 | 2 | 3 | 5 | 1.9417 | 0 | 22 |
| 0 | 0 | 1 | 2 | 4 | 8 | 2.5021 | 0 | 36 |

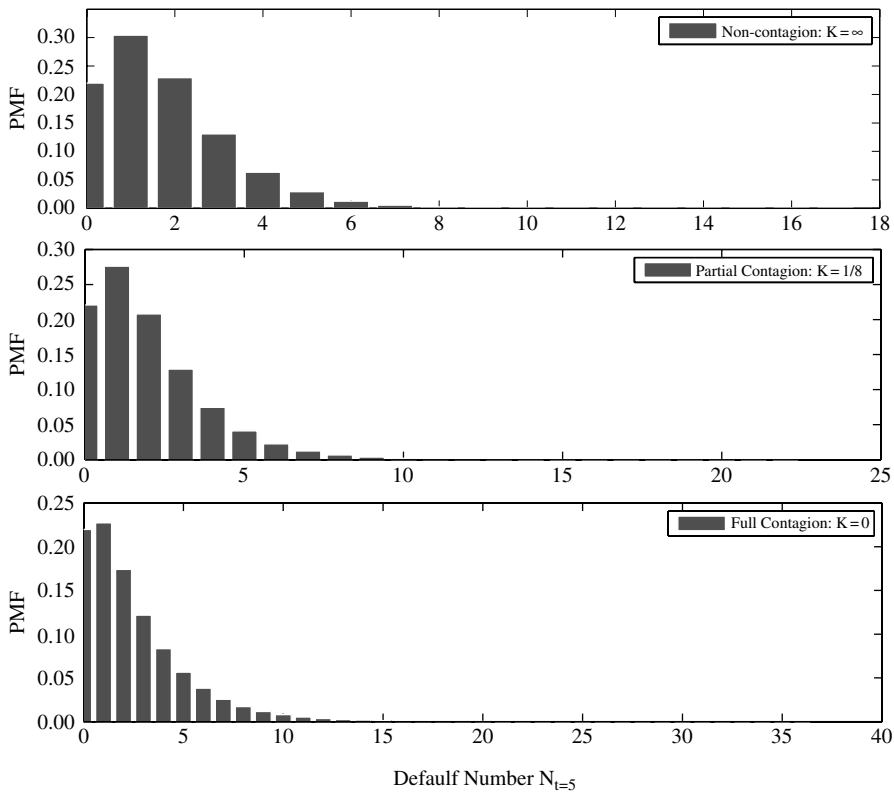


FIGURE 7: Probability mass function (PMF) of the default number $N_{t=5}$, estimated from 10^6 replications based on the parameter setting $(\delta, \rho; a, b; \ell, \bar{w}; \lambda_0) = (0.5, 0.5; 0.5, 2.0; 8.0, 2.0; 0.5)$, with homogeneous contagion thresholds $K = \infty, 1/8, 0$, respectively. The associated quantiles are reported in Table 5.

$[0, t]$ in Figure 7, and the corresponding quantiles are reported in Table 5. More specifically, cases $K = \infty, 1/8, 0$ correspond to the *non-contagion* (i.e. Case I), *partial contagion* and *full contagion* (i.e. Case II), respectively. We can clearly observe that when K decreases, the contagion would become more pronounced and the tail of losses become heavier. The system could be more susceptible to contagion risk when capital buffer K is eroded, and contagion effects magnify the content of risk. As summarised by [58], bank defaults may be driven by losses from market and credit risk (i.e. fundamental default), and bank defaults may, however,

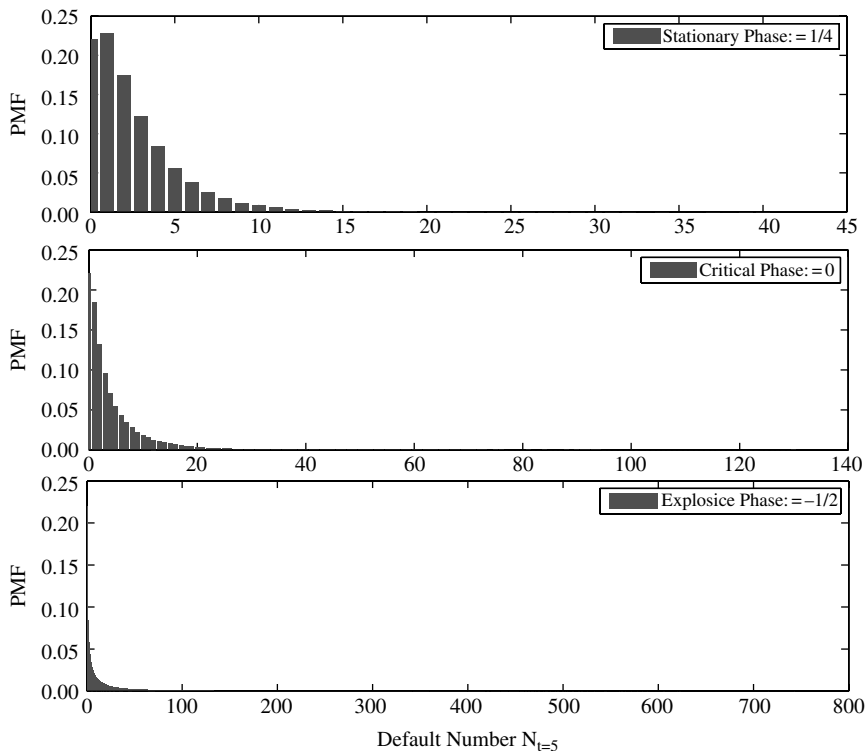


FIGURE 8: Probability mass function (PMF) of the default number $N_{t=5}$, estimated from 10^6 replications based on the parameter setting $(\delta, \rho; a, b; \bar{w}; \lambda_0) = (0.5, 0.5; 0.5, 2.0; 2.0; 0.5)$, with $\ell = 8, 4, 2$, respectively. The associated quantiles are reported in Table 6.

also be initiated by contagion as a consequence of other bank failures in the system (i.e. contagious default). The two types of default under our contagion model (i.e. the self-exciting jump sizes are not all equal to zero) are in fact mixed, and interact.

6.3. A model with explosive defaults

Contagion or feedback effects could be even further reinforced due to highly leveraged positions (e.g. complicated credit derivatives), and the resulting system thereby becomes explosive; see [38] for discussion of the impacts of financial innovations. This scenario would be extremely severe, rare but possible, that is, the entire system is unstable and near the crash boundary. Mathematically, it corresponds to the non-stationary case when $\eta < 0$ in our models. This may be due to ‘liquidity black holes’ or ‘fire sales’ of assets: these further depress prices and lead to a sharp drop in liquidity and may also cause other institutions to fail in a self-reinforcing vicious spiral [36, 37, 75, 86]. All previous examples were conducted under the stationary condition $\eta > 0$, and in fact our algorithms can also deal with non-stationary cases. In Figure 8, we offer three representative examples of $\eta = 1/4, 0$, and $-1/2$ (or $\ell = 8, 4$, and 2) for stationary, critical, and explosive phases, respectively, and the associated quantiles are reported in Table 6. In particular, $\eta = 0$ is the critical level of stability. The resulting loss distributions could present heavy tails, which might be very desirable for many regulators and practitioners.

TABLE 6: Quantiles of the default number $N_{t=5}$, estimated from 10^6 replications based on the parameter setting $(\delta, \rho; a, b; \bar{\omega}; \lambda_0) = (0.5, 0.5; 0.5, 2.0; 2.0; 0.5)$, with $\ell = 8, 4, 2$, respectively.

| ℓ | Quantile | | | | | Mean | Min | Max |
|--------|----------|-----|-----|-----|-----|---------|-----|-----|
| | 5% | 25% | 50% | 75% | 95% | | | |
| 8 | 0 | 1 | 2 | 4 | 8 | 2.4969 | 0 | 40 |
| 4 | 0 | 1 | 2 | 5 | 15 | 4.0628 | 0 | 130 |
| 2 | 0 | 1 | 4 | 16 | 73 | 15.5662 | 0 | 743 |

6.4. Other models

In fact, our models and the associated algorithms could be further extended in several other directions, which we discuss briefly due to space limitations.

- *A model with credit improvement.* In this set-up we allow for the possibility of credit improvement or relief. For example, when a big loss occurs, a rescue plan may be released such as a ‘bailout’ or a large cash injection into the system to ensure liquidity provision. This might significantly enhance the financial system in a relatively short term, and the intensity level may have an immediate decline instead of a climb, that is,

$$\lambda_{T_i} = d_i \lambda_{T_i^-}, \quad (6.3)$$

where $d_i > 0$ is a multiplier (which could be assumed to be a positive random variable). This model allows the intensity to jump in two ways, which can be simply generated by replacing (3.13) in step 4 of Algorithm 3.3 with (6.3).

- *A model with structural breaks.* A severe financial failure could make a large impact on the entire economic environment. For example, the collapse of the US investment banking giant Lehman Brothers in September 2008 marked a clear tipping point for the entire world financial market. Such a failure would immediately act on the default intensity process and cause a structural break for the entire financial system. To model this pattern, we have to go beyond the original definition of the underlying intensity process (2.2), but our algorithms can still handle it easily; that is, after each self-exciting jump, all parameters Θ can be reset afterwards to mimic a structural break. We can assign a new parameter set Θ_i immediately after the i th defaults. Θ_i could depend on the value of the size of the i th self-exciting jump X_i or even its entire history. So, the underlying intensity process (2.2) should be redefined locally based on the interarrival intensity (2.1) between two successive default times rather than globally throughout the positive real line $t \in \mathbb{R}^+$. Let us illustrate this with a simple example. Suppose there are two economic states after each self-exciting jump, one corresponding to a deteriorating economic environment and the other to an improved environment. We can use the parameter settings of Θ_1 and Θ_2 to model these two states respectively. We can choose one to be stable (i.e. the stationary case $\eta > 0$) and the other to be unstable (i.e. the non-stationary case $\eta > 0$). Then the entire system could shift between *locally stable* and *locally explosive* phases. Analysis for contagion risk based on the stability of branching processes and allowing for a shift between two phases can also be found in [27] and [38].

- *A model with multiple exogenous risk drivers.* In practice, there may be multiple risk factors, such as sector-wide or market-wide events, commonly shared by all institutions. Multi-factor models are then required for modelling intensity processes; see e.g. [54], [44], and [82]. We could use a superposition of OU intensity processes driven by different gamma processes to capture the corresponding multiple risk factors. Similarly, the superposition of OU stochastic volatility processes was proposed in [13] and [15], [16]. Accordingly, our algorithms may be extendable to this version by using the *superposition theory* of point processes [43].
- *A model with multilateral contagion.* Contagion occurs not only within one market (or system) but could also spread across different markets. For example, when the loss contagion and investors' fears occur in the options market, this can also spread to the underlying equity or futures markets on which the options are written. This type of contagion can be captured by adding *mutually exciting* jumps. As for the multivariate Hawkes process, a multi-dimensional Γ -contagion process has to be developed to capture self-contagion effects for each individual, as well as the mutual contagion effects among them.

7. Conclusion

In this paper we have introduced a new family of self-exciting jump processes whose intensities are driven by non-Gaussian OU processes, namely Lévy-driven contagion processes. Backed by the very large family of Lévy subordinators, it indeed offers much richer choices beyond the classical Hawkes process for modelling the 'contagion' of event arrivals in a continuous-time set-up in finance, economics, and many other fields. We have derived some important distributional properties of these new processes which lead to an exact simulation framework in general. In particular, we have developed exact simulation algorithms by the decomposition approach for the gamma and tempered stable cases as typical examples. The algorithms are accurate and efficient, and have been numerically verified and tested by extensive numerical experiments. We also provide applications to portfolio risk management, which again illustrate the efficiency, accuracy, applicability, and flexibility of our algorithms. As a class of reduced-form models, it could easily be extended to pricing financial derivatives, particularly multiple-name credit products (e.g. collateralised debt obligations and mortgage-backed securities). It can be employed empirically when input data are available for parameter calibration. Furthermore, it could be widely applied to many other areas, for example to describe high-frequency trading data in market microstructure, claim arrivals for an insurance portfolio, or jump propagation and disclosure dynamics in financial markets [1]. Their statistical inference and econometric analysis for this new framework, and further extensions to multi-dimensional point processes for modelling multilateral contagion, as well as further applications and empirical work for portfolio credit risk analysis, could be very interesting and meaningful topics for future research.

Appendix A. Basic distributional properties

In this section we derive some basic distributional properties such as Laplace transforms and means to characterise this new family in general. The means will also be used for validating the associated simulation algorithms. First, let us provide the Laplace transform of intensity process as follows.

Proposition A.1. (Laplace transform of intensity process.) *Under the condition $\delta > \mu_G$, i.e. $\eta > 0$, the Laplace transform of λ_{t+s} conditional on λ_t is given by*

$$\mathbb{E}[e^{-\nu\lambda_{t+s}} \mid \lambda_t] = \exp\left(-\mathcal{G}_\nu^{-1}(s)\lambda_t - \rho \int_{\mathcal{G}_\nu^{-1}(s)}^\nu \frac{\Phi(u)}{\delta u + \hat{g}(u) - 1} du\right), \quad s > 0, \tag{A.1}$$

where $\mathcal{G}_\nu^{-1}(\cdot)$ is the well-defined inverse function of

$$\mathcal{G}_\nu(x) := \int_x^\nu [\delta u + \hat{g}(u) - 1]^{-1} du.$$

The Laplace transform of the asymptotic and stationary intensity process is given by

$$\lim_{t \rightarrow \infty} \mathbb{E}[e^{-\nu\lambda_t}] = \exp\left(-\rho \int_0^\nu \frac{\Phi(u)}{\delta u + \hat{g}(u) - 1} du\right). \tag{A.2}$$

Proof. The infinitesimal generator of (λ_t, N_t, t) acting on any function $f(\lambda, n, t)$ within its domain $\Omega(\mathcal{A})$ is given by

$$\begin{aligned} \mathcal{A}f(\lambda, n, t) &= \frac{\partial f}{\partial t} - \delta\lambda \frac{\partial f}{\partial \lambda} + \rho \left\{ \int_0^\infty \left[f(\lambda + z, n, t) - f(\lambda, n, t) \right] \nu(dz) \right\} \\ &\quad + \lambda \left[\int_0^\infty f(\lambda + y, n + 1, t) dG(y) - f(\lambda, n, t) \right]. \end{aligned}$$

See [51], [52], and [56] for more details on using infinitesimal generators. Using the martingale approach similarly to [46], it is easy to obtain (A.1). Note that we have $\mathcal{G}_\nu^{-1}(t) \rightarrow 0$ when $t \rightarrow \infty$; then the Laplace transform becomes independent of the time and the initial intensity, so we have (A.2). \square

Note that the *interarrival intensity process*, i.e. the intensity process between two consecutive self-exciting jumps (excluding self-exciting jumps), is simply a Lévy-driven OU process. Hence, given the arrival times $\{T_i\}_{i=1,2,\dots}$, the Laplace transform of λ_{T_i+s} conditional on the intensity level λ_{T_i} for any fixed time s within the time period $(0, T_{i+1} - T_i)$ can be expressed more nicely as follows, by setting $\hat{g}(u) = 1$ in (A.1) to eliminate all self-exciting jumps.

Corollary A.1. (Laplace transform of the interarrival intensity process.) *Given the i th and $(i + 1)$ th arrival times T_i and T_{i+1} respectively, the Laplace transform of $\lambda_{T_i+\tau}$ conditional on λ_{T_i} is given by*

$$\mathbb{E}[e^{-\nu\lambda_{T_i+\tau}} \mid \lambda_{T_i}] = \exp\left(-\nu e^{-\delta\tau} \lambda_{T_i} - \frac{\rho}{\delta} \int_{\nu v}^\nu \frac{\Phi(u)}{u} du\right), \quad \tau \in (0, T_{i+1} - T_i).$$

The mean of point process is provided in Proposition 2.1 with the proof as follows.

Proof. The mean of N_{t+s} conditional on N_t and λ_t immediately follows by calculating

$$\mathbb{E}[N_{t+s} \mid N_t, \lambda_t] = N_t + \mathbb{E}\left[\int_s^{t+s} \lambda_u du \mid \lambda_t\right] = N_t + \int_s^{t+s} \mathbb{E}[\lambda_u \mid \lambda_t] du,$$

where

$$\mathbb{E}[\lambda_{t+s} \mid \lambda_t] = \begin{cases} \frac{\rho\mu_Z}{\eta} + \left(\lambda_t - \frac{\rho\mu_Z}{\eta}\right) e^{-\eta s} & \eta \neq 0, \\ \lambda_t + \rho\mu_Z s & \eta = 0, \end{cases}$$

which can be derived by differentiating the conditional Laplace transform (A.1). \square

Appendix B. A/R scheme for exact simulation of random variable W

Algorithm B.1. (A/R scheme for W .) The random variable W with density

$$f_W(u) = \frac{1}{C_w} \frac{\ln u}{\vartheta u - 1/\delta} \mathbf{1}_{\{1, 1/w\}}, \tag{B.1}$$

can be exactly simulated by the following A/R procedure.

(i) Generate a random variable

$$E_e = w^{-\sqrt{U_0}}, \quad U_0 \sim \mathbf{U}[0, 1]. \tag{B.2}$$

(ii) Generate a standard uniform random variable $U \sim \mathbf{U}[0, 1]$.

(iii) If

$$U \leq \frac{bE_e}{\vartheta E_e - 1/\delta},$$

then accept and set $W = E_e$. Otherwise, reject this candidate and go back to step 1.

Proof. Note that

$$\vartheta u - \frac{1}{\delta} = bu + \frac{1}{\delta}(u - 1) \geq bu, \quad u \in \left[1, \frac{1}{w}\right].$$

Then we have

$$f_W(u) = \frac{1}{C_w} \frac{\ln u}{\vartheta u - 1/\delta} \leq \frac{1}{C_w} \frac{\ln u}{bu}.$$

The density function of the envelope E_e is

$$f_{E_e}(u) = \frac{1}{E_w} \frac{\ln u}{u}, \quad E_w := \frac{1}{2} \ln^2 w, \quad u \in \left[1, \frac{1}{w}\right],$$

and the CDF is

$$F_{E_e}(u) = \left(\frac{\ln u}{\ln w}\right)^2, \quad u \in \left[1, \frac{1}{w}\right],$$

which has the analytic inverse

$$F_{E_e}^{-1}(x) = w^{-\sqrt{x}}, \quad x \in [0, 1].$$

Therefore, we have

$$\frac{f_W(u)}{f_{E_e}(u)} = \left(\frac{1}{C_w} \frac{\ln u}{\vartheta u - 1/\delta}\right) / \left(\frac{1}{E_w} \frac{\ln u}{u}\right) \leq \left(\frac{1}{C_w} \frac{\ln u}{bu}\right) / \left(\frac{1}{E_w} \frac{\ln u}{u}\right) = \frac{1}{b} \frac{E_w}{C_w} = \frac{\ln^2 w}{2bC_w} := \bar{c}_w,$$

and the acceptance condition for the A/R scheme is

$$U \leq \frac{1}{\bar{c}_w} \frac{f_W(E_e)}{f_{E_e}(E_e)} = b \frac{E_e}{\vartheta E_e - 1/\delta}.$$

□

Appendix C. A/R scheme for exact simulation of random variable V

Algorithm C.1. (*A/R scheme for V .*) The random variable V with density (4.11) can be exactly simulated via the following A/R procedure.

(i) Generate a random variable

$$E_e = \left\{ \frac{1}{2} \left[(\alpha C_w U_3 + 2) + \sqrt{(\alpha C_w U_3 + 2)^2 - 4} \right] \right\}^{1/\alpha}, \quad U_3 \sim \mathbf{U}[0, 1], \quad (C.1)$$

where

$$C_w = \frac{1}{\alpha}(w^{-\alpha} + w^\alpha - 2).$$

(ii) Generate a standard uniform random variable $U_4 \sim \mathbf{U}[0, 1]$.

(iii) If

$$U_4 \leq \frac{\beta^{1-\alpha}}{E_{e^{\alpha-1}} - E_{e^{-1-\alpha}}} \frac{1 - E_{e^{-\alpha}}}{(\kappa E_e - 1/\delta)^{1-\alpha}},$$

then accept and set $V = E_e$. Otherwise, reject this candidate and go back to step 1.

Proof. The density of V in (4.11) can be rewritten as

$$f_V(u) = \frac{1}{D_w} \frac{1}{\kappa^{1-\alpha}} \frac{1 - u^{-\alpha}}{(u - 1/(\delta\kappa))^{1-\alpha}}, \quad u \in \left[1, \frac{1}{w} \right].$$

By introducing a constant ξ such that

$$\xi \geq \frac{u^{1-\alpha}}{(u - 1/(\delta\kappa))^{1-\alpha}} \quad \text{for all } u \in \left[1, \frac{1}{w} \right],$$

we have

$$f_V(u) < \frac{1}{D_w} \frac{\xi}{\kappa^{1-\alpha}} [u^{-(1-\alpha)} - u^{-(1+\alpha)}] \quad \text{for all } u \in \left[1, \frac{1}{w} \right].$$

Since the function

$$\frac{u^{1-\alpha}}{(u - 1/(\delta\kappa))^{1-\alpha}}$$

is a strictly decreasing function of $u \in [1, 1/w]$, that is,

$$\frac{d}{du} \left[\frac{u^{1-\alpha}}{(u - 1/(\delta\kappa))^{1-\alpha}} \right] = (\alpha - 1) \frac{1}{\delta\kappa} u^{-\alpha} \left(u - \frac{1}{\delta\kappa} \right)^{\alpha-2} < 0,$$

we have $\xi \geq (\kappa/\beta)^{1-\alpha}$ for any $u \in [1, 1/w]$, and then

$$\xi \geq \max_{1 \leq u \leq 1/w} \left\{ \frac{u^{1-\alpha}}{(u - 1/(\delta\kappa))^{1-\alpha}} \right\} = \left(\frac{\kappa}{\beta} \right)^{1-\alpha}.$$

We choose E_e to be the envelope random variable with density

$$g_{E_e}(u) = \frac{1}{C_w} [u^{-(1-\alpha)} - u^{-(1+\alpha)}], \quad u \in \left[1, \frac{1}{w} \right].$$

Its CDF is

$$F_{E_e}(u) = \frac{1}{\alpha C_w}(u^{-\alpha} + u^\alpha - 2), \quad u \in \left[1, \frac{1}{w}\right],$$

which has an explicit inverse function

$$F_{E_e}^{-1}(x) = \left\{ \frac{1}{2} \left[(\alpha C_w x + 2) + \sqrt{(\alpha C_w x + 2)^2 - 4} \right] \right\}^{1/\alpha}, \quad x \in [0, 1].$$

Hence, E_e can be exactly simulated via the explicit inverse transform (C.1). Setting $\xi = (\kappa/\beta)^{1-\alpha}$, we have the *acceptance rate* (i.e. the expected number of candidates generated until one is accepted)

$$\bar{c}_w = \frac{\xi}{\kappa^{1-\alpha}} \frac{C_w}{D_w} = \beta^{1-\alpha} \frac{C_w}{D_w} \geq \frac{f_V(u)}{g_{E_e}(u)}. \quad \square$$

We have also carried out some numerical tests for Algorithm C.1 and found that it can achieve a high level of efficiency and accuracy. For example, it only takes about 7 seconds to generate 10^6 replications with percentage error 0.1% for the parameter setting $(\delta, \rho, \alpha, \beta, \theta) = (0.5, 1, 0.9, 0.2, 0.25)$.

Appendix D. Backward recursive (BR) scheme for stable index $\alpha = 1/4$

Algorithm D.1. (*Backward recursive (BR) scheme.*) To simulate one random variable of TS ($\alpha = 1/4, \beta, \theta$), we proceed as follows.

- (i) Simulate an IG random variable

$$S_2 \sim \text{IG} \left(2\theta\beta^{-1/4}\Gamma\left(\frac{3}{4}\right), 8\theta^2\Gamma^2\left(\frac{3}{4}\right) \right).$$

- (ii) Conditional on one realisation of S_2 , simulate another IG random variable,

$$S_1 | S_2 \sim \text{IG} \left(\frac{1}{2}\beta^{-1/2}S_2, \frac{1}{2}S_2^2 \right).$$

- (iii) The resulting random variable S_1 is exactly equal in distribution to TS ($\alpha = 1/4, \beta, \theta$).

Note that IG random variables can be very efficiently simulated without the A/R mechanism using the classical algorithm developed by [85]. See the proof of this algorithm and other choices of the stable index α in [50].

Appendix E. Simple stable rejection (SSR) scheme

Algorithm E.1. (*Simple stable rejection (SSR) scheme.*) To simulate one random variable $TS \sim \text{TS}(\alpha, \beta, \theta)$, we proceed as follows.

- (i) Generate a stable random variable $S(\alpha, \theta)$ via

$$S(\alpha, \theta) \stackrel{D}{=} (-\theta\Gamma(-\alpha))^{1/\alpha} \frac{\sin(\alpha U_s + \frac{1}{2}\pi\alpha)}{(\cos(U_s))^{1/\alpha}} \left[\frac{\cos((1-\alpha)U_s - \frac{1}{2}\pi\alpha)}{E_s} \right]^{(1-\alpha)/\alpha},$$

where $U_s \sim \text{U}[-\frac{1}{2}\pi, \frac{1}{2}\pi]$, $E_s \sim \text{Exp}(1)$, and they are independent.

- (ii) Generate a uniformly distributed random variable $U \sim \mathbf{U}[0, 1]$.
- (iii) If $U \leq e^{-\beta S(\alpha, \theta)}$, then accept and set $TS = S(\alpha, \theta)$. Otherwise, reject it and go back to step 1.

Acknowledgements

The authors would like to thank all reviewers for very helpful and constructive comments and suggestions. The corresponding author Hongbiao Zhao would like acknowledge the financial support from the National Natural Science Foundation of China (#71401147) and the research funds provided by Shanghai University of Finance and Economics and Shanghai Institute of International Finance and Economics.

References

- [1] ACHARYA, V. V., DEMARZO, P. AND KREMER, I. (2011). Endogenous information flows and the clustering of announcements. *Amer. Econom. Rev.* **101**, 2955–79.
- [2] AHNERT, T. AND KAKHBOD, A. (2017). Information choice and amplification of financial crises. *Rev. Financial Studies* **30**, 2130–2178.
- [3] AÏT-SAHALIA, Y. AND JACOD, J. (2009). Estimating the degree of activity of jumps in high frequency data. *Ann. Statist.* **37**, 2202–2244.
- [4] AÏT-SAHALIA, Y. AND JACOD, J. (2011). Testing whether jumps have finite or infinite activity. *Ann. Statist.* **39**, 1689–1719.
- [5] AÏT-SAHALIA, Y. AND JACOD, J. (2014). *High-Frequency Financial Econometrics*. Princeton University Press, NJ.
- [6] AÏT-SAHALIA, Y., CACHO-DIAZ, J. AND LAEVEN, R. J. (2015). Modeling financial contagion using mutually exciting jump processes. *J. Financial Econometrics* **117**, 585–606.
- [7] AÏT-SAHALIA, Y., LAEVEN, R. J. AND PELIZZON, L. (2014). Mutual excitation in Eurozone sovereign CDS. *J. Econometrics* **183**, 151–167.
- [8] ASMUSSEN, S. AND GLYNN, P. W. (2007). *Stochastic Simulation: Algorithms and Analysis*. Springer, New York.
- [9] AZIZPOUR, S., GIESECKE, K. AND SCHWENKLER, G. (2018). Exploring the sources of default clustering. *J. Financial Econometrics* **129**, 154–183.
- [10] BACRY, E., DELATTRE, S., HOFFMANN, M. AND MUZY, J.-F. (2013). Modelling microstructure noise with mutually exciting point processes. *Quant. Finance* **13**, 65–77.
- [11] BARNDORFF-NIELSEN, O. E. (1997). Normal inverse Gaussian distributions and stochastic volatility modelling. *Scand. J. Statist.* **24**, 1–13.
- [12] BARNDORFF-NIELSEN, O. E. (1998). Processes of normal inverse Gaussian type. *Finance Stoch.* **2**, 41–68.
- [13] BARNDORFF-NIELSEN, O. E. (2001). Superposition of Ornstein–Uhlenbeck type processes. *Theory Prob. Appl.* **45**, 175–194.
- [14] BARNDORFF-NIELSEN, O. E. AND SHEPHARD, N. (2001). Modelling by Lévy processes for financial econometrics. In *Lévy Processes*, eds O. E. Barndorff-Nielsen, S. I. Resnick, and T. Mikosch, pp. 283–318. Birkhäuser, Boston.
- [15] BARNDORFF-NIELSEN, O. E. AND SHEPHARD, N. (2001). Non-Gaussian Ornstein–Uhlenbeck-based models and some of their uses in financial economics. *J. R. Statist. Soc. B* **63**, 167–241.
- [16] BARNDORFF-NIELSEN, O. E. AND SHEPHARD, N. (2002). Econometric analysis of realized volatility and its use in estimating stochastic volatility models. *J. R. Statist. Soc. B* **64**, 253–280.
- [17] BARNDORFF-NIELSEN, O. E. AND SHEPHARD, N. (2003). Integrated OU processes and non-Gaussian OU-based stochastic volatility models. *Scand. J. Statist.* **30**, 277–295.
- [18] BARNDORFF-NIELSEN, O. E. AND SHEPHARD, N. (2003). Realized power variation and stochastic volatility models. *Bernoulli* **9**, 243–265.
- [19] BARNDORFF-NIELSEN, O. E., JENSEN, J. L. AND SØRENSEN, M. (1998). Some stationary processes in discrete and continuous time. *Adv. Appl. Prob.* **30**, 989–1007.
- [20] BOWSHER, C. G. (2007). Modelling security market events in continuous time: intensity based, multivariate point process models. *J. Econometrics* **141**, 876–912.
- [21] BRÉMAUD, P. AND MASSOULIÉ, L. (1996). Stability of nonlinear Hawkes processes. *Ann. Prob.* **24**, 1563–1588.

- [22] BRÉMAUD, P. AND MASSOULIÉ, L. (2002). Power spectra of general shot noises and Hawkes point processes with a random excitation. *Adv. Appl. Prob.* **34**, 205–222.
- [23] BRIX, A. (1999). Generalized gamma measures and shot-noise Cox processes. *Adv. Appl. Prob.* **31**, 929–953.
- [24] BROADIE, M. AND KAYA, Ö. (2006). Exact simulation of stochastic volatility and other affine jump diffusion processes. *Operat. Res.* **54**, 217–231.
- [25] BRUNNERMEIER, M. K. (2009). Deciphering the liquidity and credit crunch 2007–2008. *J. Econom. Perspectives* **23**, 77–100.
- [26] BRUNNERMEIER, M. K. AND PEDERSEN, L. H. (2009). Market liquidity and funding liquidity. *Rev. Financial Studies* **22**, 2201–2238.
- [27] CACCIOLI, F., SHRESTHA, M., MOORE, C. AND FARMER, J. D. (2014). Stability analysis of financial contagion due to overlapping portfolios. *J. Bank. Finance* **46**, 233–245.
- [28] CAI, N., SONG, Y. AND CHEN, N. (2017). Exact simulation of the SABR model. *Operat. Res.* **65**, 931–951.
- [29] CARR, P., GEMAN, H., MADAN, D. B. AND YOR, M. (2003). Stochastic volatility for Lévy processes. *Math. Finance* **13**, 345–382.
- [30] CENTANNI, S. AND MINOZZO, M. (2006). A Monte Carlo approach to filtering for a class of marked doubly stochastic Poisson processes. *J. Amer. Statist. Assoc.* **101**, 1582–1597.
- [31] CHEN, N. AND HUANG, Z. (2013). Localization and exact simulation of Brownian motion-driven stochastic differential equations. *Math. Operat. Res.* **38**, 591–616.
- [32] CHEN, Z., FENG, L. AND LIN, X. (2012). Simulating Lévy processes from their characteristic functions and financial applications. *ACM Trans. Model. Comput. Simul.* **22**, 14:1–14:26.
- [33] CHHIKARA, R. AND FOLKS, L. (1989). *The Inverse Gaussian Distribution: Theory, Methodology, and Applications*. Marcel Dekker, New York.
- [34] CONT, R. (2001). Empirical properties of asset returns: stylized facts and statistical issues. *Quant. Finance* **1**, 223–236.
- [35] CONT, R. AND TANKOV, P. (2004). *Financial Modelling with Jump Processes*. CRC Press, Boca Raton.
- [36] CONT, R. AND WAGALATH, L. (2013). Running for the exit: distressed selling and endogenous correlation in financial markets. *Math. Finance* **23**, 718–741.
- [37] CONT, R. AND WAGALATH, L. (2016). Fire sales forensics: measuring endogenous risk. *Math. Finance* **26**, 835–866.
- [38] CORSI, F., MARMI, S. AND LILLO, F. (2016). When micro prudence increases macro risk: the destabilizing effects of financial innovation, leverage, and diversification. *Operat. Res.* **64**, 1073–1088.
- [39] COX, D. R. (1955). Some statistical methods connected with series of events. *J. R. Statist. Soc. B* **17**, 129–164.
- [40] COX, D. R. (1972). Regression models and life-tables. *J. R. Statist. Soc. B* **34**, 187–220.
- [41] CRANE, R. AND SORNETTE, D. (2008). Robust dynamic classes revealed by measuring the response function of a social system. *Proc. Nat. Acad. Sci. USA* **105**, 15649–15653.
- [42] CREDITRISK⁺ (1997). *CreditRisk⁺: A Credit Risk Management Framework*. Credit Suisse First Boston International, New York.
- [43] DALEY, D. J. AND VERE-JONES, D. (2003). *An Introduction to the Theory of Point Processes*, vol. I: *Elementary Theory and Methods*. Springer, New York.
- [44] DAS, S. R., DUFFIE, D., KAPADIA, N. AND SAITA, L. (2007). Common failings: how corporate defaults are correlated. *J. Finance* **62**, 93–117.
- [45] DASSIOS, A. AND EMBRECHTS, P. (1989). Martingales and insurance risk. *Stoch. Models* **5**, 181–217.
- [46] DASSIOS, A. AND ZHAO, H. (2011). A dynamic contagion process. *Adv. Appl. Prob.* **43**, 814–846.
- [47] DASSIOS, A. AND ZHAO, H. (2013). Exact simulation of Hawkes process with exponentially decaying intensity. *Electron. Commun. Probab.* **18**, 1–13.
- [48] DASSIOS, A. AND ZHAO, H. (2017). A generalised contagion process with an application to credit risk. *Int. J. Theor. Appl. Finance* **20**, 1–33.
- [49] DASSIOS, A. AND ZHAO, H. (2017). Efficient simulation of clustering jumps with CIR intensity. *Operat. Res.* **65**, 1494–1515.
- [50] DASSIOS, A., QU, Y. AND ZHAO, H. (2018). Exact simulation for a class of tempered stable and related distributions. *ACM Trans. Model. Comput. Simul.* **28**, 20:1–20:21.
- [51] DAVIS, M. H. (1984). Piecewise-deterministic Markov processes: a general class of non-diffusion stochastic models. *J. R. Statist. Soc. B* **46**, 353–388.
- [52] DAVIS, M. H. (1993). *Markov Models and Optimization*. Chapman & Hall/CRC, London.
- [53] DEVROYE, L. (2009). Random variate generation for exponentially and polynomially tilted stable distributions. *ACM Trans. Model. Comput. Simul.* **19**, 1–20.
- [54] DUFFIE, D. AND GÄRLEANU, N. (2001). Risk and valuation of collateralized debt obligations. *Financial Analysts Journal* **57**, 41–59.
- [55] DUFFIE, D., ECKNER, A., HOREL, G. AND SAITA, L. (2009). Frailty correlated default. *J. Finance* **64**, 2089–2123.

- [56] DUFFIE, D., FILIPOVIC, D. AND SCHACHERMAYER, W. (2003). Affine processes and applications in finance. *Ann. Appl. Prob.* **13**, 984–1053.
- [57] EBERLEIN, E., MADAN, D., PISTORIUS, M. AND YOR, M. (2013). A simple stochastic rate model for rate equity hybrid products. *Appl. Math. Finance* **20**, 461–488.
- [58] EISENBERG, L. AND NOE, T. H. (2001). Systemic risk in financial systems. *Manag. Sci.* **47**, 236–249.
- [59] ELSINGER, H., LEHAR, A. AND SUMMER, M. (2006). Risk assessment for banking systems. *Manag. Sci.* **52**, 1301–1314.
- [60] EMBRECHTS, P., LINIGER, T. AND LIN, L. (2011). Multivariate Hawkes processes: an application to financial data. *J. Appl. Prob.* **48A**, 367–378.
- [61] ERRAIS, E., GIESECKE, K. AND GOLDBERG, L. R. (2010). Affine point processes and portfolio credit risk. *SIAM J. Financ. Math.* **1**, 642–665.
- [62] GENÇAY, R., DACOROGNA, M., MULLER, U. A., PICTET, O. AND OLSEN, R. (2001). *An Introduction to High-Frequency Finance*. Academic Press, San Diego.
- [63] GIESECKE, K., KAKAVAND, H. AND MOUSAVI, M. (2011). Exact simulation of point processes with stochastic intensities. *Operat. Res.* **59**, 1233–1245.
- [64] GIESECKE, K., LONGSTAFF, F. A., SCHAEFER, S. AND STREBULAEV, I. (2011). Corporate bond default risk: a 150-year perspective. *J. Financial Econometrics* **102**, 233–250.
- [65] GLASSERMAN, P. (2003). *Monte Carlo Methods in Financial Engineering*. Springer, New York.
- [66] GLASSERMAN, P. AND LIU, Z. (2010). Sensitivity estimates from characteristic functions. *Operat. Res.* **58**, 1611–1623.
- [67] GORDY, M. B. (2000). A comparative anatomy of credit risk models. *J. Bank. Finance* **24**, 119–149.
- [68] GORDY, M. B. (2003). A risk-factor model foundation for ratings-based bank capital rules. *J. Financial Intermediation* **12**, 199–232.
- [69] HAINAUT, D. AND DEVOLDER, P. (2008). Mortality modelling with Lévy processes. *Insurance Math. Econom.* **42**, 409–418.
- [70] HAWKES, A. G. (1971). Point spectra of some mutually exciting point processes. *J. R. Statist. Soc. B* **33**, 438–443.
- [71] HAWKES, A. G. (1971). Spectra of some self-exciting and mutually exciting point processes. *Biometrika* **58**, 83–90.
- [72] HAWKES, A. G. AND OAKES, D. (1974). A cluster process representation of a self-exciting process. *J. Appl. Prob.* **11**, 493–503.
- [73] HOFERT, M. (2011). Sampling exponentially tilted stable distributions. *ACM Trans. Model. Comput. Simul.* **22**, 1–11.
- [74] KANG, C., KANG, W. AND LEE, J. M. (2017). Exact simulation of the Wishart multidimensional stochastic volatility model. *Operat. Res.* **65**, 1190–1206.
- [75] KRISHNAMURTHY, A. (2010). How debt markets have malfunctioned in the crisis. *J. Econom. Perspectives* **24**, 3–28.
- [76] KYPRIANOU, A. (2006). *Introductory Lectures on Fluctuations of Lévy Processes with Applications*. Springer, Berlin.
- [77] LARGE, J. (2007). Measuring the resiliency of an electronic limit order book. *J. Financial Markets* **10**, 1–25.
- [78] LEE, S. S. AND HANNIG, J. (2010). Detecting jumps from Lévy jump diffusion processes. *J. Financial Econometrics* **96**, 271–290.
- [79] LEWIS, P. A. AND SHEDLER, G. S. (1979). Simulation of nonhomogeneous Poisson processes by thinning. *Naval Res. Logist. Quart.* **26**, 403–413.
- [80] LI, H., WELLS, M. T. AND CINDY, L. Y. (2008). A Bayesian analysis of return dynamics with Lévy jumps. *Rev. Financial Studies* **21**, 2345–2378.
- [81] LI, L. AND LINETSKY, V. (2014). Time-changed Ornstein–Uhlenbeck processes and their applications in commodity derivative models. *Math. Finance* **24**, 289–330.
- [82] LONGSTAFF, F. A. AND RAJAN, A. (2008). An empirical analysis of the pricing of collateralized debt obligations. *J. Finance* **63**, 529–563.
- [83] MADAN, D. B. AND SENETA, E. (1990). The variance gamma (V.G.) model for share market returns. *J. Business* **63**, 511–524.
- [84] MADAN, D. B., CARR, P. P. AND CHANG, E. C. (1998). The variance gamma process and option pricing. *Europ. Finance Rev.* **2**, 79–105.
- [85] MICHAEL, J. R., SCHUCANY, W. R. AND HAAS, R. W. (1976). Generating random variates using transformations with multiple roots. *Amer. Statistician* **30**, 88–90.
- [86] MORRIS, S. AND SHIN, H. S. (2004). Liquidity black holes. *Rev. Finance* **8**, 1–18.
- [87] NICOLATO, E. AND VENARDOS, E. (2003). Option pricing in stochastic volatility models of the Ornstein–Uhlenbeck type. *Math. Finance* **13**, 445–466.

- [88] POTERBA, J. M. AND SUMMERS, L. H. (1988). Mean reversion in stock prices: evidence and implications. *J. Financial Econometrics* **22**, 27–59.
- [89] QU, Y., DASSIOS, A. AND ZHAO, H. (2019). Exact simulation for tempered stable distributions. Working paper, London School of Economics.
- [90] QU, Y., DASSIOS, A. AND ZHAO, H. (2019). Exact simulation of gamma-driven Ornstein–Uhlenbeck processes with finite and infinite activity jumps. Working paper, London School of Economics.
- [91] ROSIŃSKI, J. (2001). Series representations of Lévy processes from the perspective of point processes. In *Lévy Processes*, eds O. E. Barndorff-Nielsen, S. I. Resnick, and T. Mikosch, pp. 401–415. Birkhäuser, Boston.
- [92] ROSIŃSKI, J. (2007). Tempering stable processes. *Stoch. Process. Appl.* **117**, 677–707.
- [93] RYDBERG, T. H. AND SHEPHARD, N. (2000). A modelling framework for the prices and times made on the NYSE. In *Nonlinear and Nonstationary Signal Processing* (Isaac Newton Institute Series), eds W. Fitzgerald, R. Smith, A. Walden, and P. Young. Cambridge University Press.
- [94] SATO, K.-I. (1999). *Lévy Processes and Infinitely Divisible Distributions*. Cambridge University Press.
- [95] SCHOUTENS, W. AND CARIBONI, J. (2010). *Lévy Processes in Credit Risk*. John Wiley, Chichester.